# Improvements in reproducibility, throughput and capacity of microfluidic acoustic trapping systems

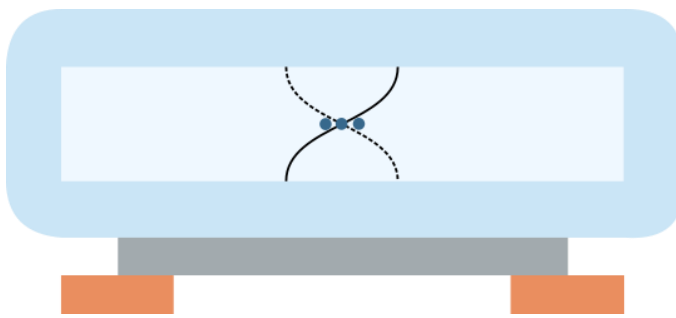

Daniel Glifberg

2016

Master's Thesis in

Biomedical Engineering

Faculty of Engineering LTH

Department of Biomedical Engineering

Supervisor: Mikael Evander

Examiner: Thomas Laurell


LUND UNIVERSITY

# Table of Contents

**List of abbreviations**

| | |
|---|---|
| **BVD** | Butterworth-Van Dyke |
| **$F_{grad}$** | Optical gradient force |
| **$F_{scatt}$** | Optical scattering force |
| **μ-TAS** | Micro-Total Analysis System |
| **μCP** | Micro-Contact printing |
| **MALDI-TOF MS** | Matrix assisted laser desorption/ionization mass spectrometry |
| **MEMS** | Microelectromechanical systems |
| **PDMS** | Poly(dimethylsiloxanes) |
| **PRF** | Primary Radiation Force |
| **SRF** | Secondary Radiation Force |

**List of variables & constants**

| | |
|---|---|
| **ϱ** | Density |
| **P** | Pressure |
| **η** | Dynamic Viscosity |
| **v** | Velocity |
| **$D_h$** | Hydraulic diameter |
| **Re** | Reynolds number |
| **A** | Area |
| **CM** | Clausius-Mossotti factor |
| **K** | Isentropic bulk modulus |
| **ϰ** | Compressibility |
| **z** | Acoustic Impedance |
| **R** | Reflection coefficient |
| **T** | Transmission coefficient |
| **$f_{1-2}$** | Contrast factors |
| **ν** | Kinematic viscosity |
| **$Q_m$** | Mechanical quality factor |
| **$F_r$** | Series resonance frequency |
| **Y** | Admittance |
| **G** | Conductance |

# Abstract

Acoustic trapping is a novel technology that allows for microfluidic sample preparation and pretreatment. The aim of this text is to give the reader a general insight in microfluidics with a focus on acoustic trapping. One of the next steps in the development of acoustic trapping is to promote commercialization of the technology which requires that similar devices can be manufactured reproducibly. In this thesis the fabrication steps of acoustic trapping systems were investigated to increase the reproducibility of device manufacture. The fabcrication steps were refined by improving the soldering of the trapping devices and by developing a new method for attaching the capillaries to the trapping chip. This new method resulted in more reproducible devices but also led to a decrease in overall trapping capacity for a given voltage over the piezoelectric element.

Another matter of investigation in this thesis was to improve the capacity of trapping systems. The relationship between channel dimensions, size of the piezoelectric element and capacity was investigated. It was found that a combination of larger transducers and channels the capacity could be more than quadrupled.

# Sammanfattning

Akustisk infångning är en relativt ny teknik som tillåter behandling av biomedicinska prover i ett mikrofluidiskt system. Målet med den här uppsatsen är att ge läsaren en introduktion till mikrofluidik med ett fokus på akustisk infångning. För att möjliggöra en kommersiell utveckling av akustiska infågningssystem måste system med samma design också ha likvärdig prestanda. Ett av huvudmålen i uppsatsen är att förbättra reproducerbarheten i tillverkningen av system för akustisk infångning vilket undersöktes genom att vidareutveckla och testa olikas sätt att konstruera enheterna. En ny metod för att fästa den mikrofluidiska kanalen mot ultraljudsgivaren utvecklades vilket ökade reproducerbarheten men samtidigt minskade infångningskapaciteten.

I uppsatsen undersöktes också huruvida kapaciteten kunde förbättras. Sambandet mellan kanalstorlek, givare storlek och kapacitet var parametrarna som undersöktes. Försöken visade att en större kanal tillsammans med större givare kunde öka kapaciteten med mer än fyra gånger det ursprungliga värdet.

# Populärvetenskaplig Sammanfattning

**Förbättringar i reproducerbarhet och kapacitet av akustiska mikrofluidiska infångningssystem**

*Vad är akustisk infångning?*

Arbetet i den här uppsatsen är fokuserat på mikrofluidiska system som med hjälp av ultraljud kan fånga in celler och små partiklar. Mikrofluidik är ett fält som innefattar tekniker där man hanterar små flöden i mycket små kanaler. Principen för akustisk infångning bygger på att en stående våg av ultraljud bildas i en mikrofluidisk kanal. Ultraljudet påverkar vätskan i kanalen vilket gör att det bildas krafter som i sin tur påverkar cellerna eller partiklarna i vätskan. Detta får cellerna och partiklarna att klumpas ihop och fångas på ett specifikt ställe längs med kanalen. Ultraljudet bildas av en piezoelektrisk kristall, vilket är ett material som ändrar form när en elektrisk spänning appliceras. Genom att variera den elektriska potentialen med hög frekvens kan kristallen fås att vibrera snabbt och bilda ultraljud.

Den här tekniken kan användas inom sjukvården för tillämpningar där prover av blod, urin eller andra kroppsvätskor behöver analyseras. Oftast är man intresserad av antingen cellerna i proverna eller av själva vätskan. Med akustisk infångning kan man på ett snabbt och skonsamt sätt t.ex. extrahera celler från den omgivande plasman genom att fånga in cellerna. Cellerna kan sedan behandlas antingen direkt i den akustiska fällan eller med andra metoder. Dessa steg är viktiga inom diagnos av många olika former av sjukdomar från malaria till cancer.

*Arbetet*

I arbetet ingick att studera och förbättra system för akustisk infångning genom att öka reproducerbarhet i tillverkningsprocessen. Detta innebar att förbättra montering och tillverkning av infångningssystemen. Olika sätt att förbättra kapaciteten undersöktes också genom att konstruera nya system där parametrarna på de aktiva komponenterna varierades, och hur dessa ändringar påverkade kapaciteten kartlades. Det visade sig att kapaciteten kunde ökas med mer än fyra gånger den ursprungliga genom att använda större kanaler och ultraljudsgivare.

Arbetet som utförts är viktigt för att föra akustisk infångningstekniken närmare produktion genom att titta på reproducerbarhet och kapacitet. Båda är viktiga parametrar för tillämpningar av tekniken.

# Acknowledgements

I'd like to thank my supervisor Mikael Evander for his guidance in this project and my examiner Thomas Laurell for introducing me to the project to begin with. I would also like to thank everyone at the department of biomedical engineering that helped me with various tasks during the project, especially Axel Tojo, Carl Johannesson and Marc Isaksson. I would also like to thank Paulina Bryl-Gorecka for assisting with the flow cytometry. I wish to extend special gratitude to my parents, Hans Glifberg and Åsa Liljegren-Glifberg, and to my brother Jonathan Glifberg, for always supporting me throughout these years of studying.

# Introduction

It is well-known and researched that waves that propagate through a medium apply a pressure on receiving bodies due to the formation of radiation forces. Radiation forces are created by all forms of waves when they interact with an object in the path of wave propagation. This includes both mechanical waves, e.g. acoustic, and electromagnetic waves, e.g. optical (light) waves. Harnessing radiation forces has been attempted in vastly different fields ranging from biomedical and biophysical applications to astronautics. In astronautics the electromagnetic radiation pressure produced by solar rays is investigated by scientist to be used to propel space crafts using vast solar sails. Electromagnetic radiation forces have also been employed on completely different size scales. For instance in biophysics, electromagnetic radiation forces have been used for optic manipulation of particles and cells. One such technology, popularly referred to as optical tweezers, works by forming an optical radiation force by focusing a laser beam through a lens of high numerical aperture [1]. The focused laser beam will scatter on the bodies of semitransparent targets and generate forces that can be used for manipulation and trapping. Mechanical waves, for instance acoustic waves, will in the same manner as electromagnetic waves generate radiation pressure on objects in the field of wave propagation. Acoustic waves are longitudinal waves that travels by compression and expansion of the material. There are also mechanical waves that move by oscillations perpendicular to the direction of propagation and these are called transverse waves. Radiation forces originating from acoustic, and especially ultrasonic sources, has been a subject of scientific research since the first half of the 19$^{th}$ century. However the study of acoustic radiation forces didn't take off as a field of research until the beginning of the 20$^{th}$ century when Lord Rayleigh observed a phenomena he called "the pressure of vibrations" [2]. The observations made by Lord Rayleigh have since then been extensively researched and widely employed in biomedical applications, ranging from biosensors to medical imaging and gene delivery [3]. In this master thesis the radiation forces produced by longitudinal ultrasonic standing waves is used for acoustic trapping in microfluidic glass capillaries. Acoustic trapping is a non-invasive and non-contact trapping technique that levitates and retains cells or particles at a specific location in a confined environment to achieve pre-fractionation, population specific cell studies, enrichment or separation/filtering [4].

## Acoustic trapping for microfluidic based sample preparation

In general, one of the weaknesses of microfluidic-based bioanalysis is sample preparation. For many microfluidic technologies and chip designs, it has proven to be a great challenge to include conversion of a raw sample with low concentrations of analytes to a sample ready for analysis on chip [5]. Following sample preparation the concentration of analyte has to be over the limit of detection for the specific

method of analysis and the sample must be in a state that is easy to handle in the microfluidic system.

Standard sample preparation requires complicated and time consuming pretreatment procedures including steps like centrifugation, enrichment, cell lysis and others. A sample preparation process chain is illustrated in figure 1 b. One of the reasons these steps are difficult to perform on chip is that they involve processing large volumes of fluid compared to the nanoliter flows usually present in microfluidic devices. Another challenge for sample preparation in microfluidics is that the size of bio-particles can span several orders of magnitude (figure 1 a). The analyte in question can be a protein, bacteria, virus, eukaryotic cell or different kinds of biomarkers. These are often present in very low quantities in a highly complex sample fluid i.e. blood, urine or other types of media [6].

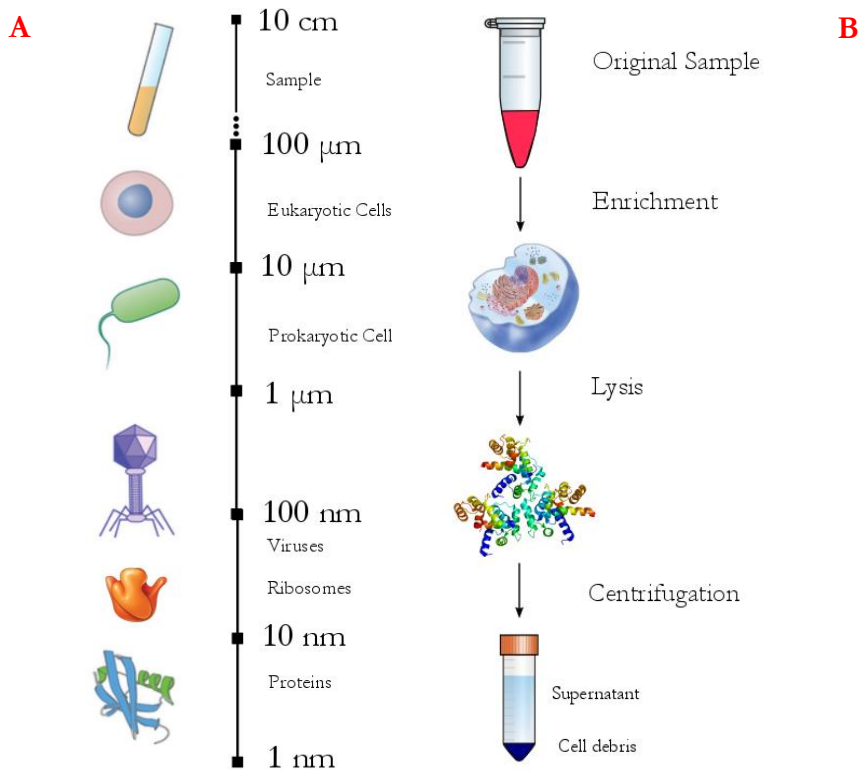


Figure 1 A). The size of bio particles that are interesting for biomedical analysis range in several order of magnitudes, from eukaryotic cells themselves to the intracellular proteins within them and the extracellular proteins that surround them. In this image DNA is not included since it is very small in in one dimension but can be extremely long. B). This flow-chart depicts common steps included in sample preparation. The sample is first often enriched from the original source. If the analyte is intracellular the enriched sample can be lysed and centrifuged. The extracted analyte is then located in the supernatant that can be used in analysis. Sometimes even the supernatant needs to be processed prior to analysis.

The goal with all sample preparation is to extract the analyte to increase the specificity of an assay. Extracting the analyte is achieved by removing the complex surrounding medium and at the same time concentrating the analyte [7]. The results and quality of all bioanalytical assays depend to some extent on the initial sample preparation. Thus sample preparation is a key component in all forms of bioanalysis. Continuous advances in bioanalytical assays have enabled detection of lower and lower amounts of analytes at higher throughput. As the sensitivity and throughput of assays increases, a greater demand is put on faster and more accurate sample pretreatment and analyte extraction. Acoustic trapping is a promising technology for sample pretreatment and has the potential to address some of the issues with microfluidic-based sample preparation presented above. Acoustic trapping has been used in pretreatment steps for mass spectrometry, bead based immunoassays, continuous cell culture studies and other bioanalytical technologies [8].

The work presented in this thesis outlies a study on acoustic trapping that can be divided into two parts. The first part is focused on increasing reproducibility in the fabrication process of acoustic traps while the second part focuses on increasing to the capacity of acoustic traps.

## Part I: Improving reproducibility in fabrication of acoustic trapping systems

Reproducibility is a key component for both large and small scale production of bioanalytical devices. It is important to be able to ensure that every device will work in the same fashion and produce similar results. The fabrication method of acoustic traps was investigated with the goal to identify the steps that introduce variations between acoustic trapping devices. Once identified, the goal was to minimize the variations to increase reproducibility and overall robustness of the fabrication process. There are three major steps in fabrication of the acoustic trapping devices which all introduce variations between different devices. These steps are; forming a piezoelectric element, soldering of the element to a PCB to form an ultrasonic transducer and adhering a microchannel (glass capillary) to the transducer using an acoustic coupling layer. The reproducibility of each step was assessed using electrical impedance measurements.

## Part II: Improving capacity and throughput of acoustic trapping systems

Part II of this thesis focused on increasing the capacity and the throughput of acoustic traps. The capacity is a measurement of the total amount of analyte (particles) a device can hold at the trapping site. Throughput is a measurement of the volume per unit of time the device can handle and still perform as desired. In this thesis the influence of

size of the piezoelectric element on the trapping capacity was investigated to see if a larger element would produce higher capacity traps. The influence of the size in regards to the capillary on trapping capacity was also tested. The standard size of capillaries used in the trapping devices had a cross-sectional area of 0.2 mm x 2 mm. Larger capillaries with the dimensions 0.2 mm x 4 mm and 0.4 mm x 4 mm respectively, were investigated to see if that would allow for an increase in capacity. The capillary with 0.4 mm of height means that the device should resonate at the first overtone, which in theory should produce two set of nodes for trapping. It was investigated whether operating the traps at the first overtone would increase the capacity or not. The methods developed in part I of this thesis were used to fabricate the traps for part II, with modifications made where it was required.

# Background

The background to this thesis is divided into chapters. Chapter I will mainly serve as an introduction to general microfluidics, Chapter II will deal with microfabrication whereas Chapter III will give an introduction to cell and particle trapping and finally Chapter IV will focus on acoustic theory and especially acoustofluidics and the technology of acoustic trapping.

# Chapter I

## Microfluidic Theory and Concepts

The field of microfluidics emerged as expertise from several scientific fields met and cooperated to develop microscale platforms that could perform standard analytical tasks present in fields ranging from chemical analysis to molecular biology. These microscale platforms were fabricated using methods derived from the semiconductor industry [9]. The goal of microfluidics is to improve established methods of analysis by downscaling the analysis process to the micro domain and develop new methods of analysis that are not possible on the macroscale. Going from macro- to microscale means that less materials and regents are required for analysis and since distances are smaller reaction speeds increase. Microfluidic devices are also usually referred to as μ-TAS (micro-total analytical system), bio-MEMS (bio microelectromechanical systems) or Lab-on-A-Chip. The long term goal with a lab-on-a-chip devices is to allow processes that today require an entire lab, including both manual and machine processes, to take place on a single chip. Ideally in such micro devices all the steps necessary for analysis should take place on the chip including sample preparation, sample handling between analysis steps, sample treatment and analyte detection. And as was mentioned before, sample preparation can be particularly hard to realize on chip.

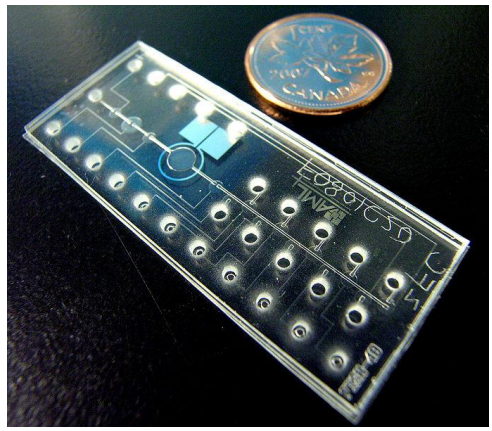

Figure 2. The chip illustrated in this figure is an automated and integrated microchip that incorporates a reagent multiplexer, a cell chamber with an integrated thin-film heater, and a peristaltic pump. The image also the relative size of a microfluidic device compared to a coin. The device was fabricated in silicon and glass where the chambers and connections were formed by several etching step. Obtained from Wikimedia Commons.

Microfluidic chips often have several compartments where each compartment performs one or several tasks and together they can treat and analyze the sample. An example is featured in figure 2.

When downscaling from the macroscale to the microscale, several changes occur in the dominating physical parameters which result in; (1) fluids behave differently, (2) the surface area to volume ratio increases, (3) surface tension and viscosity becomes dominant and (4) diffusion becomes much more prominent. If you imagine water flowing through rivers, taps or large pipes, you'd have an intuitive understanding of how the water would behave. In macroscale flows, inertia of the fluid determines how the fluid behaves. Inertia introduces turbulent effects that manifest themselves as vortexes and eddies that continuously fold and stretch fluid streamlines, which as a result mixes the fluid. At microfluidic flows viscosity and surface tension dominates over inertia, which creates a predictable non-turbulent flow referred to as laminar flow [10]. The behavior of fluids at the microscale can be predicted by using a number of dimensionless numbers, a few of which will be presented below.

**Laminar flow**

A fluid is a continuous body which is best described by vector fields that specifies the value of a parameter (e.g. velocity) at every point in the fluid. The velocity vector field of a Newtonian fluid (viscosity is linearly related to strain rate) is described using the Navier-Stokes equations [11]. The Navier-Stokes equation is written as

Eq 1. $$\rho\left(\frac{dV}{dt} + V \cdot \nabla \mathrm{V}\right) = -\nabla \mathrm{p} + \eta \nabla^2 V + f$$

where, ρ is the density of the fluid, p is the pressure field, η is the viscosity of the fluid and f is the body force/forcing term. The body force represents all the bulk forces acting on the liquid including electrostatic and gravitational forces. Non-dimensionalization of the Navier-Stokes equations by employing the characteristic velocity ($V_c$) and the hydraulic dimension/diameter of the channel ($D_H$) yields the Reynolds equation. The hydraulic diameter is used to perform calculations for non-circular fluidic channels as if they were circular. The solution to the Reynold equation is called the Reynolds number (Re) and it compares the vicious forces ($f_v$) to the inertial forces ($f_i$) of the liquid and indicates whether the flow is laminar or turbulent [10].

Eq 2.
$$Re = \frac{f_i}{f_v} = \frac{\rho V_c D_H}{\eta}$$

A Reynolds number much less than one (1»Re) is said to be in the Stokes flow regime (creeping flow), while Reynold numbers above ~2000 are defined as turbulent flows. Reynolds numbers between 1 and 2000 are said to be in the laminar domain [12]. Inertial effects, i.e. the amount and magnitude of swirls and eddies, increases with increasing Reynolds numbers. The magnitude of turbulence that flows of different Reynolds numbers exhibit with an object in the path of the streamlines are illustrated in figure 3.

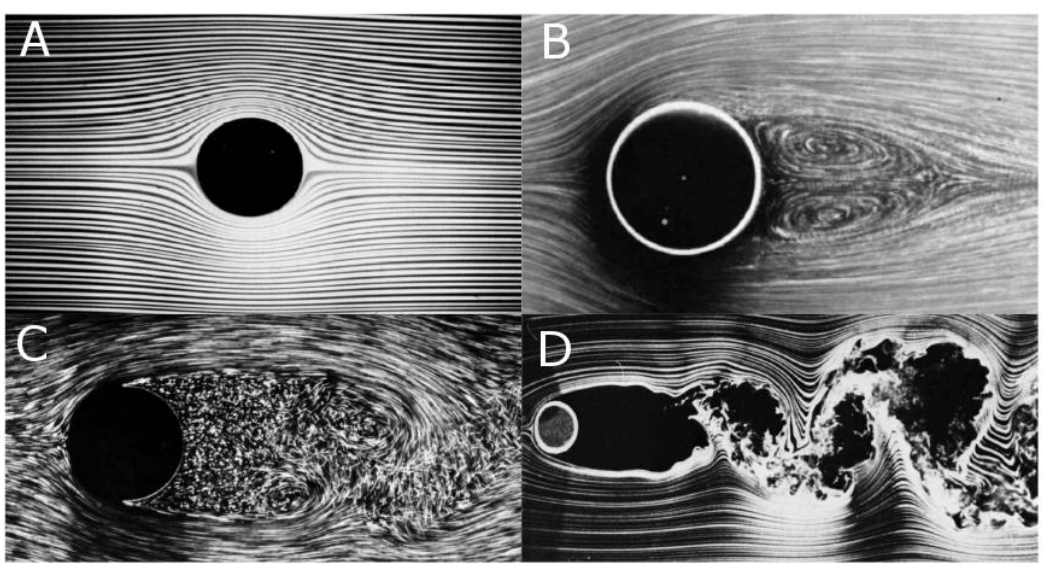


Figure 3 A). Creeping flow with a Re of less than 1. B). Laminar flow with Re = 26, small vortices visible but no breakdown of laminar streamlines. C). Re = 2000 and the streamlines are deteriorating. D). Re = 10000 the flow is the turbulent regime and chaotic mixing folds the streamlines. These images were obtained from [13].

Even though inertial effects usually are absent in microfluidic systems several approaches have been developed that specifically use higher flowrates and/or curving channels to achieve greater Re numbers. High Re numbers in microfluidics are usually undesirable as it leads to mixing and requires high flowrates. High Re numbers can be taken advantage of by clever design to gain inertial effects e.g. dean flow and hydrodynamic lift forces [14]. These inertial effects can be used to separate particles due to size and focus particles into fixed positions in the channels.

**Mixing in microfluidic devices**

The advantages of the laminar flow in microfluidic systems are mainly an increase in control, predictability and repeatability that the laminar flow provides. Since there is a low amount of turbulence in laminar flow, the convective mixing component is minimal. Thus under laminar flow conditions two liquids will flow alongside each other without lateral mixing. Mixing will only occur due to diffusion of molecules at the interfaces of the two liquids, and the liquids can be seen as flowing parallel layers.

A number of different mixers have been developed that utilize the fast diffusion rates at the microscale. An example is the T-mixer which consists of two inlets that come together and form a single channel where parallelization of the flows of fluids occur. Between the fluids there will be concentration gradients and diffusive mixing takes place as the fluid travel along the channel [15]. Another more advanced diffusive mixer is the herringbone mixer that rotates and folds streamlines by having groves at the walls of the channels. The folding of the fluid increases mixing by shortening the distance of diffusion between streamlines [16].

**Transport of fluids in microfluidic systems**

The most common way to achieve propulsion of fluids through microfluidic systems is by pressure driven flow or electro-osmosis [17]. In addition to pressure and electric fields, other methods of moving fluids within microfluidic circuits include forces arising due to wetting of surfaces i.e. capillary driving forces and flows driven by gradients in interfacial tensions i.e. Marangoni flows [18].

Pressure-driven flow

Pressure-driven flow is achieved by using precise syringe pumps manufactured for microfluidic applications. The behavior of pressure-driven flow in circular channels is explained by the Hagen-Poisseullie equation. This equation share similarities with Ohm's law for electric circuits, where the voltage drop, resistance and current, can be seen as analogous to the pressure drop, hydraulic resistance and the fluid flow [19]. Assuming steady-state of a pressure driven flow in a circular channel, then the velocity vector from the Naiver-Stokes equation shows that fluid in the center of the channel flows faster than fluid closer towards the channel walls. This gives rise to a characteristic parabolic flow profile which can be found in pressure driven flows [19].

The parabolic flow profile can be a major disadvantage since it introduces dispersion, which can affect the resolution of the detection signal. Another disadvantage with pressure-driven flow it that it requires moving parts, which is undesirable in most biomedical applications. The main advantages with using pressure-drive flows are high control of flow rates, that it works on any type of fluid and isn't dependent on surface interactions [17].

**Stokes Drag**

A force will be generated upon a particle if it is moved through a viscous medium or if the medium is moved relative to the particle. This occurs for instance in trapping applications as the particle is held stationary and the fluid passes by. Assuming laminar flow, a homogenous medium, smooth spherical particles and no particle interaction, then the viscous drag force can be calculated using Stoke's law,

Eq 3. $$F_d = 6\pi\eta\alpha v$$

where $\eta$ is the dynamic viscosity, $\alpha$ is the radius of the particle and v is the velocity of the medium. The drag force scales with the radius of the particle which means that the force decreases only marginally with particle size compared to other forces in trapping applications that normally scale with the volume and surface area of the particle. The result is that the drag force becomes a limiting factor in many trapping applications.

# Chapter II

## Fabrication of microfluidic devices

Initially when the field of microfluidics emerged, the fabrication methods available for realizing microstructures were adopted from the semiconductor and microelectronic industries and involved use of materials typical to those industries, i.e. silicon and glass. A trend in fabrication of microfluidic devices is to move towards materials that are cheaper, have easier fabrication steps and are more biocompatible than the materials used in the semiconductor industry. Most of the newly adopted materials are some sort of polymers. In this thesis prefabricated glass capillaries will be used as microfluidic channels and thus the process of semiconductor and glass manufacturing will not be discussed. One way of using polymers to produce microstructures is called soft lithography and will be used in a step called contact printing for the reproducibility parts of this thesis.

**Soft Lithography**

A group of techniques used to generate micro patterns using an elastomeric materials for replica molding have been collectively named soft lithography and utilizes materials like poly(dimethylsiloxanes) (PDMS) or other polymers like silicones or polyurethanes, for fabrication of microstructures [20].

The soft lithography process begins with the generation of a master which holds the microstructure. The master can be produced in many different ways, but most commonly a master is made using semiconductor fabrication methods or milling. Once the master is created the microstructure defined in the master is replicated by using for instance PDMS. A PDMS base is mixed with a curing agent to initiate cross-linking of pre-polymers and the mixture is then poured over the master and cured at an elevated temperature (~60-80 C) for 1-2 hours [21]. In liquid form, PDMS easily adapts to and replicates the patterns of the master and it retains these features during curing. PDMS has low surface energy which is beneficial since the cured structure can be easily pealed of from the master without damaging either the replicated structure or the master itself [22]. After fabrication the PDMS replica is usually sealed against glass by air plasma treatment to create channels. The soft lithography process is illustrated in figure 4.

Micro-contact printing (μCP)

PDMS structures can also be used for Micro-Contact Printing (μCP) in which a PDMS replica is formed from a master and used to print molecules or structures on surfaces. In μCP a solution containing particles or a specific surface chemistry is applied to the stamp and then transferred by contacting the stamp to the surface [23].

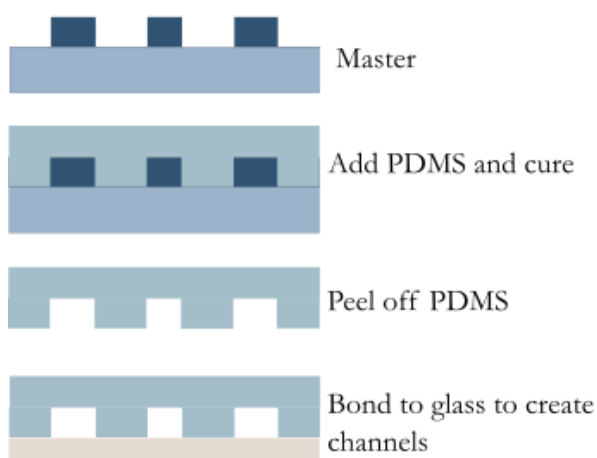


Figure 4. A soft lithography master can be created in many ways but most common is by UV-lithography. The PDMS base is mixed, degassed and poured over the master. Curing takes place in an elevated temperature after which the PDMS is peeled off. To form channels, the PDMS structure can be bounded to glass.

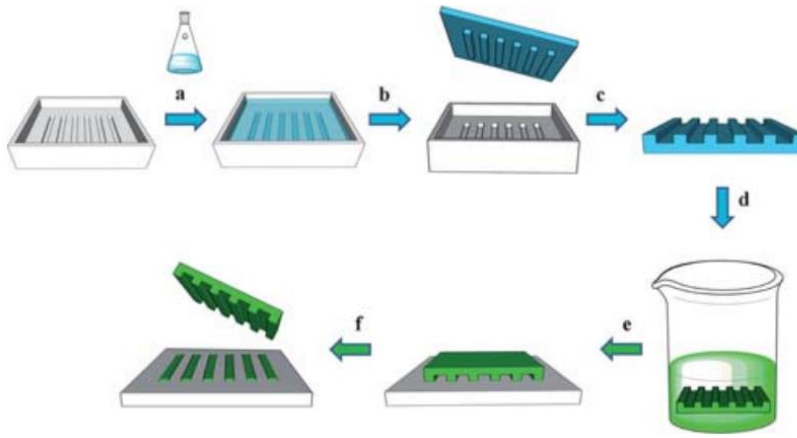


Figure 5. The essential steps of μCP. a) A master is generated and a PDMS (blue) mixture is poured into it. b) The PDMS stamp is cured and then peeled off. c) Any modifications to the stamp are made. d) The stamp is "inked" which means it is introduced to the surface that should be transferred. e) the stamp is placed into contact with the receiving surface. f) After the ink has transferred the stamp is removed. Obtained from [24].

The stamp is held against the other surface from 30 s to several minutes before being released. The pattern generated on the new surface upon release of the PDMS stamp is determined by the raised bas-relief pattern of the stamp. Using PDMS in μCP allows for transfer of a surface chemistry and geometry with a resolutions lower than 100 nm [25]. In this thesis, PDMS stamping will be investigated as a means to transfer a controlled amount of adhesive for contacting a microchannel to acoustic transducers for acoustic trapping devices. The μCP process is illustrated in figure 5.

# Chapter III

## Microfluidic Cell and Particle Trapping

Several technologies have been developed for trapping of cells or particles at defined positions in microfluidic systems with the goal to carry out tasks such as sample preparation, single cell studies, enrichment and separation/filtering [26]. Microfluidic cell trapping is of great interest in biomedical applications and can be used for fields including oncology, stem cell research and cardiology. By isolating cells from their surrounding medium, microfluidic trapping could help in diagnosis of many diseases. For instance in malaria, trapping of infected blood cells can speed up diagnosis, in cancer for sorting out circulating tumor cells and various other diseases by trapping infected cells in body fluid samples [27, 28]. The mechanism of particle and cell trapping is derived from specific physical principles including forces from optical, electrical, magnetic, hydrodynamic and acoustic sources [29]. How these techniques achieve trapping will be briefly reviewed in this section as well as their applications. Acoustic trapping, which is the focus of this thesis, will be explained in detail in chapter IV of this background.

**Hydrodynamic cell trapping**

The defining features of hydrodynamic trapping technologies is that they utilizes the geometry of the channels and forces from the flow of fluids to reposition and trap particles and cells at specific sites without the use of external fields [30]. One strategy of hydrodynamic trapping is to use the inertial effects at slightly increased Re to provide lift forces and equilibrium positions to focus particles at certain positions in the channel and trap the particles using micro vortices. By designing the geometry of the channels to include protuberances at the places of equilibrium positions the particles are made to enter the cavities where they are trapped by the vortices [31]. Quantitative studies of single cells can be made in isolated hydrodynamic trapping arrays (figure 6). The technology works by having laminar flow lines carry the cell into an array of traps formed by pockets of PDMS. Once a cell has occupied a trap it will block further flow into the pocket and thus diverting the follow of cells to other traps in the array [32]. Such an array can be a vital tool for improving single cell analysis experiments. There exist numerous other approaches to hydrodynamic trapping, however they utilize many of the same principles as those described previously.

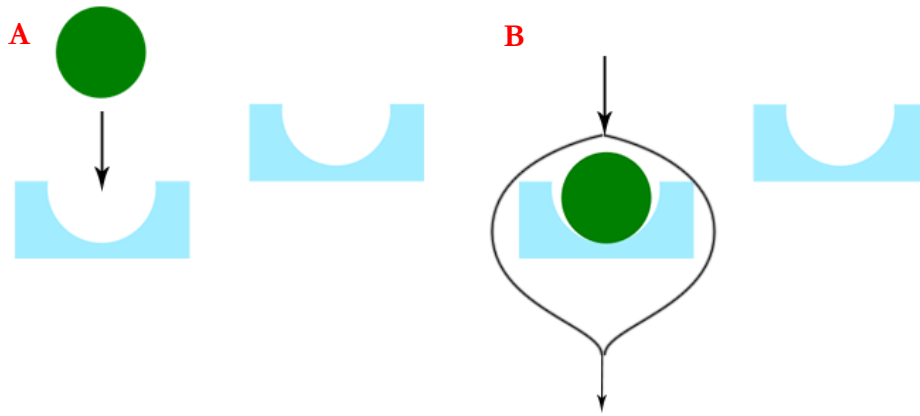


Figure 6. A) Illustration of a parallel hydrodynamic trapping array. The laminar streamlines carriy a cell towards a trap. B) As the cell enters the trap it blocks further flow into the trap and diverts the stream lines. This ensures only one cell enters each trap.

**Dielectrophoretic cell trapping**

A dielectrophoretic (DEP) force arises when polarizable particles are subjugated to an inhomogeneous electric field. The DEP force can be used to induce movement (dielectrophoresis) and for non-contact trapping of particles and cells since the forces exerted on the particles are unsymmetrical. The equation describing the DEP force contains a parameter called the Clausius–Mossotti (CM) factor. The frequency of an applied AC field will influence the CM factor depending on the relative polarizability of the particle in comparison to the medium. If the CM>0, the DEP force will be positive (p-DEP), and if the CM<0, the DEP force will be negative (n-DEP) [29]. In p-DEP the particle will be attracted towards the regions with greater field strength and in n-DEP the particle will be pulled towards the region with weaker field strength [33]. Both p-DEP and n-DEP have been used for dielectrophoretic trapping. Different designs of DEP traps have been implemented in microfluidic devices to achieve trapping with varying numbers of electrodes, positioning and geometry. An example of a 3D-electrode configuration for dielectrophoretic trapping is the extruded quadrupole trap [34]. This trap has 4 posts as electrodes, which are extruded from the floor of the microfluidic channel (figure 7).

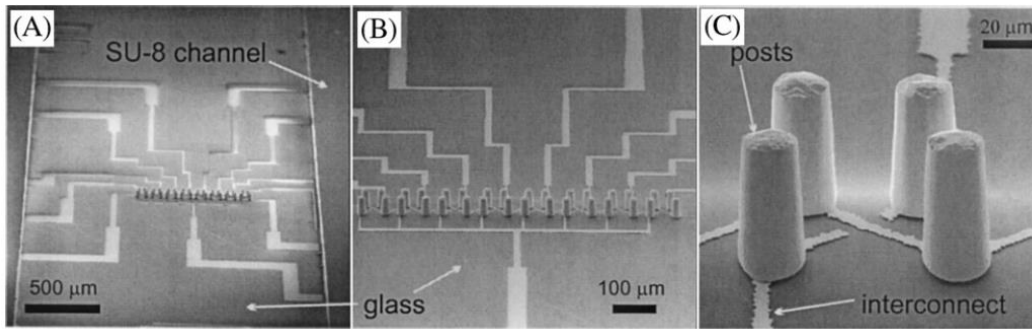


Figure 7. A) 8 extruded quadrupole traps in an array in a SU-8 channel. B) Close up of an entire array. C) Close up of one of the traps in the array with the extruded electrodes. This figure was obtained from [34].

**Optical cell trapping**

Optical tweezers were briefly mentioned in the introduction to this thesis and have been used extensively in biophysical applications for DNA and motor protein studies. In optical trapping, a laser beam is focused using a high numerical aperture microscope objective [35]. A particle close to the focus of the laser beam will experience a net force acting towards the focus of the laser beam due to scattering of indecent photons (figure 8). The primary optical force can be deconstructed into two secondary forces; one called the scattering force ($F_{scatt}$) acting in the direction of light propagation and another force called the gradient trapping force ($F_{grad}$) acting in accordance to the light gradient of the laser beam [36]. The scattering force emerges as photons from the laser beam transfer their momentum to the bead and if the laser beam is isotropic then all of the forces will cancel each other out except in the direction of light propagation. The electromagnetic field in an optical trap is inhomogeneous (due to the gradient) and dielectric particles will be polarized. Interaction between the induced dipoles and the inhomogeneous field creates the gradient trapping force. For a stable trap the requirements of $F_{grad} > F_{scatt}$ must be met or the scattering force will push the particle out of the trap. A large $F_{grad}$ is required to overcome the scattering force which can be achieved by having a steep light gradient generated by powerful high numerical aperture objectives.

Optical trapping has been used to characterize the movement pattern of motor proteins to map step size and distance moved per unit of ATP consumed by the protein by specifically controlling the interaction between the motor protein and its substrate [37]. Optical trapping has also been used for measuring interacting forces between erythrocytes and virus coated beads and the forces produced by RNA polymerase during transcription of DNA and many other applications [35]. In figure 9 a, cell trapped using optical trapping is shown.

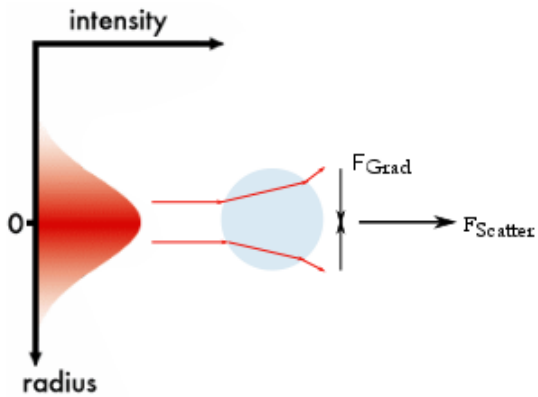


Figure 8. The gradient force acts towards the highest intensity region of the laser. The scattering force acts in the direction of light propagation due to absorption of momentum from photons. The red lines show the refraction of the light rays as they hit the transparent particle.

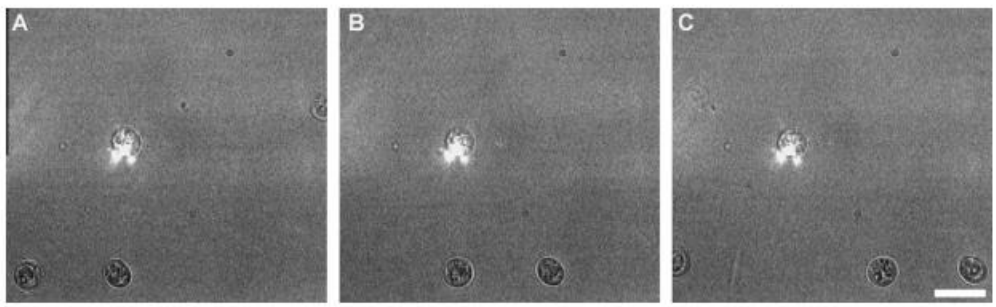


Figure 9. Optical trapping of a *Trachydiscus minutrus* cell (bright spot). The microscope stage is moved in images A-C. Cells not affected by the optical trap can be seen flowing past in the bottom part of the images. This figure was obtained from [38].

# Chapter IV

## Acoustics and Acoustofluidics

The field dedicated to studying acoustics in microfluidic applications is called acoustofluidics. In acoustofluidics, acoustic radiation forces and acoustic streaming components are employed to achieve particle manipulation on the microscale. The two major applications of acoustofluidics is separation and trapping. The motion imposed on a particle as a result of the acoustic radiation forces is called acoustophoresis. In this chapter of the background, basic acoustic theory required to understand the forces behind acoustic manipulation will be presented.

The initial acoustic theory described herein can be found in the classical book on acoustics by Kinsler [39]. One way of representing an acoustic longitudinal wave is that of a pressure field, where the oscillations occur in a continuous body of fluid of liquid or gas. The pressure variations travel through the body by compression and rarefaction of the medium, which produces forces that act on bordering regions, introducing additional compression and expansion. By these mechanisms the acoustic wave propagates. Acoustic waves can be represented by other fields describing for instance parameters like the displacement of the medium or the velocity of the displacement. An acoustic wave has to fulfill the wave equation which for pressure is defined as

Eq 4.
$$\nabla^2 p = \frac{1}{c^2}\frac{\delta^2 p}{\delta t^2}$$

where c is the speed of sound and p is the pressure field . The speed of sound can be determined by using the Newton-Laplace equation,

Eq 5.
$$c = \sqrt{\frac{K}{\rho}} = \frac{1}{\sqrt{\kappa\rho}}$$

where K is the isentropic bulk modulus, ρ is the density and κ is the compressibility of the medium. Transmission and reflection of acoustic waves occurs at the boundary between two mediums when a propagating acoustic wave reaches the interface. The amplitude and intensity of the reflected and transmitted acoustic waves, relative the incident wave, depends on the acoustic impedance and the speed of sound in the mediums as wells the angle of incidence towards the boundary (figure 10).

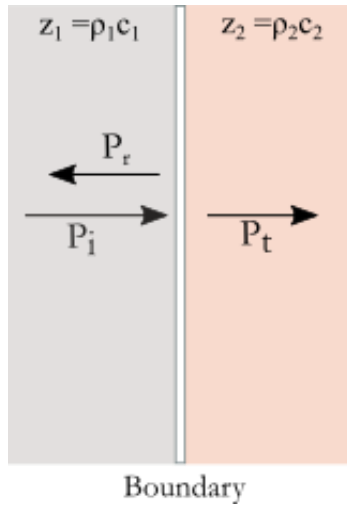


Figure 10. An incident wave ($P_i$) travels in a material with the acoustic impedance of $z_1$. It strikes a material with the acoustic impedance $z_2$. At the boundary a reflected wave ($P_r$) and transmitted wave ($P_t$) are generated. The amount of reflected and transmitted acoustic energy depends on the acoustic impedance of the two materials.

An incident pressure wave (pi) striking the boundary will generate a transmitting wave (pt) and a reflected wave (pr) as illustrated in figure 10. If you assume normal incidence and account for the boundary conditions of continuity of the acoustic pressure and continuity of normal component of velocity, then an expression for the reflection and transmission can be created. If the boundary conditions are fulfilled, then the pressure divided by the particle velocity gives

Eq 6. $$\frac{p_i + p_r}{v_i + v_r} = \frac{p_t}{v_t}$$

For a plane wave the *specific* acoustic impedance is (the sign depends on direction of wave propagation)

Eq 7. $$z = \pm\frac{p}{v}$$

The acoustic impedance is a measurement of the resistance a system imposes on an acoustic flow when an acoustic pressure wave is applied. Inserting eq 7 in eq 6 yields

Eq 8. $$z_1 \frac{p_i + p_r}{p_i - p_r} = z_2$$

Eq 8 can be rewritten to gain the reflection coefficient and transmission coefficients

Eq 9. $$R = \frac{z_2 - z_1}{z_2 + z_1}$$

Eq 10. $$T = \frac{2z_2}{z_2 + z_1}$$

These equations tell us that for materials with similar acoustic impedances a lot of transmission of acoustic energy takes place and if two materials have large differences in acoustic impedance, a lot of the acoustic energy is reflected. For a more thorough explanation of this theory, the reader is referred to the work by Kinsler et al. presented in the introduction to this chapter.

**Standing Waves**

Acoustic trapping takes place in a microfluidic channel. The channel can be regarded as a confined space where the interface between the channel walls and outside makes up the boundary conditions for the channel. As was demonstrated, there will be transmissions and reflections at these boundaries if we introduce an acoustic pressure wave. Standing waves are generated by the phase interference between indecent/transmitted and reflected waves. A simple acoustic plane wave traveling from one boundary to the other side of the channel, can be described by the equation

Eq 11. $$p(x,t) = p_0 \sin(\omega t - kx)$$

where $p_0$ is the pressure amplitude, ω is the angular frequency and k is the wavenumber. Assuming complete reflection of this wave at the boundary generates an identical wave running in the opposite direction. The reflected wave will be superimposed with the incident wave resulting in a total wave field

Eq 12. $$p_{tot}(x,t) = p_0 \sin(\omega t - kx) + p_0 \sin(\omega t + kx) = 2p_0 \sin(\omega t)\cos(kx)$$

The resulting standing wave will have locations with much greater amplitude than the original wave, called antinodes, and locations with almost no acoustic field, called nodes. At the walls, the acoustic pressure will always be maximum and thus there will always be a pressure anti-node at the walls. Frequencies that generate standing wave patterns are called resonance frequencies and are characterized by low input impedance, i.e. at those frequencies it is easy to put energy into the system. Frequencies where it is hard to add energy to the system (high input impedance) are called anti-resonance frequencies. There is an infinite number of resonance frequencies and anti-frequency for a system. The lowest order is called the fundamental frequency (1 st harmonic) and higher order resonance frequencies are referred to as overtones of the fundamental frequency. The standing wave pattern generated by the fundamental frequencies and a few overtones is shown in figure 11.

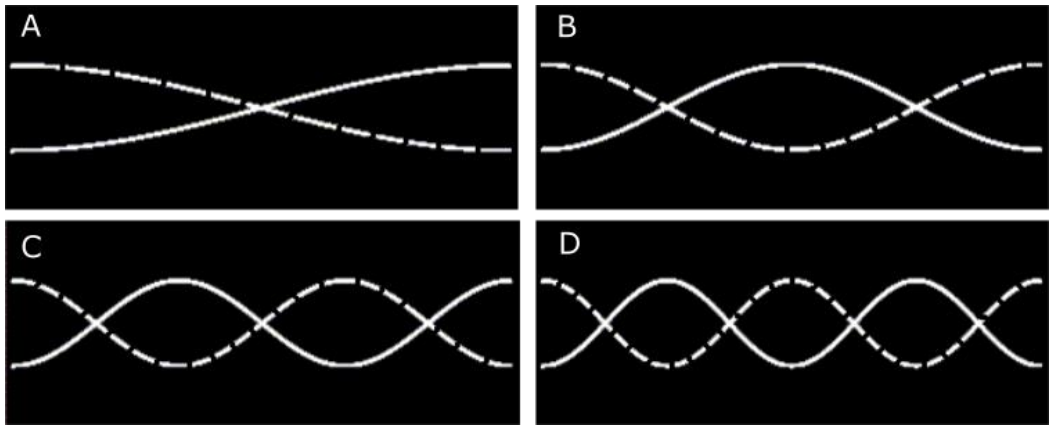


Figure 11. The acoustic pressure from a sine wave between two completely reflecting walls is illustrated. Higher order of resonance frequencies have increasing number of nodes and anti-nodes. A) The first harmonics occur when L (channel dimension) = $\lambda/2$. There is a pressure node in the center and pressure anti-nodes at the walls, B) the second harmonics (1st overtone) occur when L = $\lambda$, C) The third harmonics (2nd overtone) occurs when L = $3\lambda/2$ and D) the fourth harmonics (3rd overtone) occurs when L = $2\lambda$.

Increasing order of harmonics/overtones will have additional whole numbers of half wavelengths in the standing wave, thus increasing the number of nodes and antinodes. When actuating an acoustic system such that all the parts of the system move together at the same frequency is called an eigenmode. The frequency of an eigenmode is called the eigenfrequency.

**The Primary Radiation force**

Particles exposed to acoustic waves will experience a radiation force as mentioned in the introduction to the thesis. The radiation force depends on the interaction of the acoustic fields with the particle and have been named the direct or primary radiation force (PRF). The equation used to describe the primary radiation force was devised by Gor'kov in 1962,

Eq 13.
$$F_{PRF} = -\Delta V \left( \frac{f_1}{2\rho c^2} \langle p^2(r,t) \rangle_{\mathrm{T}} - \frac{3}{4} \rho f_2 \langle v^2(r,t) \rangle_{\mathrm{T}} \right)$$

where the equation applies for a particle with the volume V, in a fluid with the density $\rho$ and c being the speed of sound in the medium [40]. The terms $f_1$ and $f_2$ are called the contrast factors and compare the material parameters of the medium to those of the particle,

Eq 14.
$$f_1 = 1 - \frac{\rho c^2}{\rho_p c_p^2} = 1 - \frac{\beta_p}{\beta}$$

Eq 15.
$$f_2 = \frac{2(\rho_p - \rho)}{2\rho_p + \rho}$$

Where β stands for the compressibility, the subscript p refers to the particle and the parameters without a subscripted p are constants for the medium. Mannerberg showed in his doctoral thesis that the equation derived by Gor'Kov can be rewritten into a form where the force depends on either only the acoustic pressure or just the velocity fields for a particle much smaller than the wavelength [41]. For a plane wave (Eq 11) the equation presented by Mannerberg would assume the following form in the axial direction:

Eq 16.
$$F_{PRF} = -\frac{V\beta}{4} p_0^2 k \left(f_1 + \frac{3f_2}{2}\right) \sin(2kx)$$

This equation generates an acoustic field with a sinusoidal shape. The pressure and velocity fields will have points with zero amplitude (nodes) and maximum amplitude (anti-nodes) defined by the variables in the wave equation. The PRF focuses particles with compressibility lower than the medium towards the pressure nodes as is illustrated in figure 12. Bubbles and particles with greater compressibility than the medium are instead focused towards the velocity nodes. A sinusoidal acoustic standing wave with a wavelength that corresponds to the half channel width, will have pressure nodes at the center of the channel and velocity nodes as the sides of the channel.

**Secondary Radiation Force**

Shortly after Rayleighs description of the pressure of vibrations in the beginning of the 20th century, Vilhelm Bjerknes published his findings that showed that in addition to the PRF, there were forces acting between particles themselves in an acoustic field [42]. These forces have been denoted as the Bjerkne forces or secondary radiation force (SRF). The SRF only arises when particles get close to each other and are formed due to scattering of the acoustic field between the particles. Assuming a plane wave, then an equation describing the resulting SRF between two particles with the same radius can be written as,

Eq 17.
$$F_{SRF} = 4\pi\alpha_p^6 \left( \frac{(\rho_p - \rho)^2 (3\cos^2\theta - 1)}{6\rho d^4} v^2(x) - \frac{\omega^2 \rho (\beta_\rho - \beta)^2}{9d^2} p^2(x) \right)$$

where α is the radius of the particle, d is the distance between the center of the particles, ρ is the density, p is the pressure field, v is the velocity field, θ is the angle between the centerline of the particles and direction of the sound field and β is the compressibility of the particle and medium respectively [43]. This equation consists of two terms, where the left term can assume both positive and negative values depending on the positioning of the particle relative to the sound field, while the right

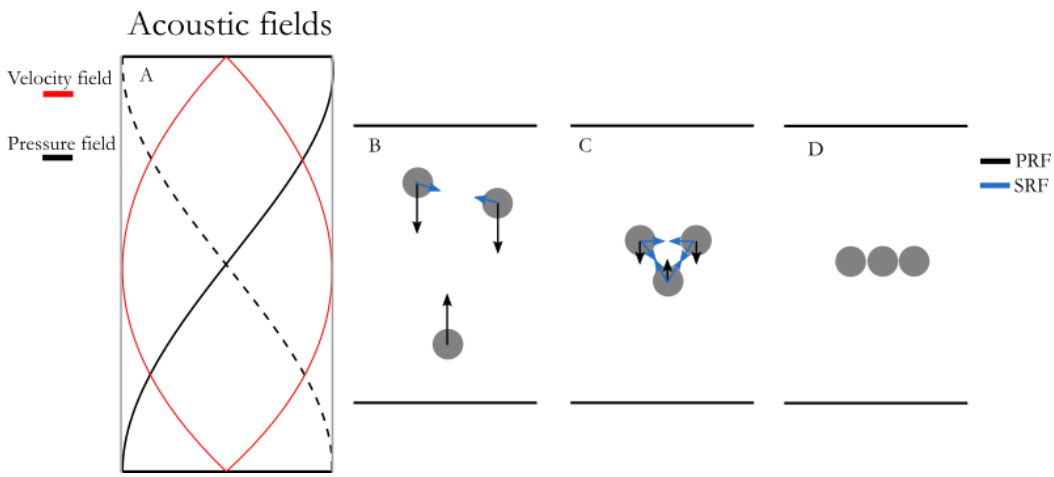


Figure 12. A) Pressure wave in a closed channel with a wavelength corresponding to L = λ/2, where L is the channel dimension, has a node in the center of the channel and anti-nodes at the side-walls. B) Particles in the channel will experience a PRF (black) focusing them towards the pressure node. The particles will also experience a SRF (blue) acting between them. C) The particles form a cluster due to the SRF. D) The particles align at the nodal plane. The forces have been omitted for clarity.

term is always positive. As was discussed above a particle can be moved towards either the velocitynodes or the pressure nodes by the PRF. The left term in the SRF vanishes for particles at the velocity nodes where particles that are more compressible than the medium gather. In the same manner, the right term vanishes at the pressure node, where cells and particles that are less compressible than the medium gather. At other places than the nodes, the angle θ determines if the force is positive or negative. The PRFs and SRFs influence on particles in a channel is illustrated in figure 12.

**Acoustic Streaming**

A fluid exposed to a sound field displays a pattern of vortices or time-independent circumvolutions (rolls) of the fluid called acoustic streaming. The vortices are created due to absorption of energy by the fluid from the acoustic fields [44]. Acoustic streaming can arise by friction between a channel wall and the medium [45]. Acoustic streaming occurs in confined geometries with standing waves (as in acoustic trapping) and the attenuation takes place in a viscous boundary layer, called the Stokes layer, close to the channel wall. The thickness of the boundary layer can be expressed as

Eq 18.

$$\delta = \sqrt{\frac{2\nu}{\omega}}$$

Where ν is the kinematic viscosity and ω is the angular frequency [46]. Fluid within the boundary layer will have a steady rotational flow that carries through to the bulk fluid, inducing streaming in the medium as depicted in figure 13.

The force generated by the fluidic drag on a particle in an acoustic streaming field can be expressed from Stoke's law (Eq 3)

Eq 19. $$F_{STR} = 6\pi\eta\alpha v_{STR}$$

where $\alpha$ is the radius of the particle, $v_{STR}$ is the streaming velocity and $\eta$ is the dynamic viscosity of the medium. The streaming velocity can be written as

Eq 20. $$v_{STR} = \Psi \frac{v_a^2}{c}$$

where $\Psi$ is a parameter that depends on the geometry of the fluidic confinement (channel), c is the speed of sound in the medium and $v_a$ is the amplitude of the velocity field [46]. Acoustic streaming is important in trapping applications as it helps with moving particles towards trapping sites. However the streaming also creates drag on particles which can overcome the trapping forces and disrupt acoustic trapping.

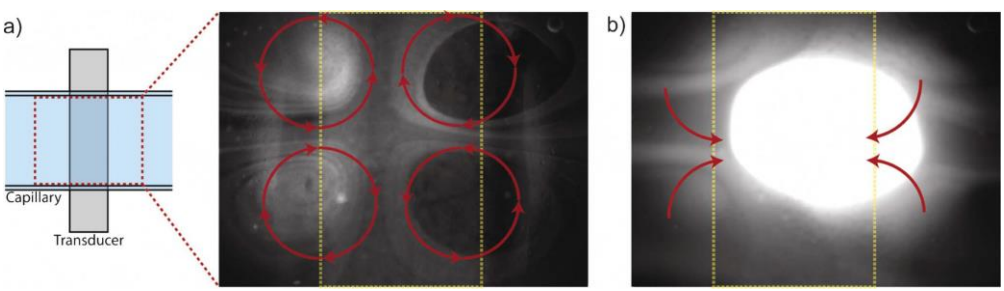


Figure 13 A) Acoustic streaming patterns generated by a transducer for acoustic trapping. 490 nm particles are used to visualize the streaming patterns. The yellow lines represent the location of the transducer. B) Higher concentrations of particles lead to trapping at the pressure node. Particles outside of the trapping region are stilled affected by the streaming. Particles are transported to the trapping site by the streaming. This figure was obtained from [47]

**Acoustic trapping**

Prior to the observations made by Rayleigh and Bjerknes on the effects of the acoustic radiation forces, the effects of these forces in a confined space were witnessed in an experiment performed by August Kundt [48]. The experiment became known as Kundt's tube experiment and consisted of an air filled tube with fine particles of saw dust. A standing acoustic wave was introduced into the tube using a moving piston. A primary radiation force arose when resonance was achieved and the particles gathered at the pressure nodes in the tube and were repelled from the velocity nodes. The PRF and SRF are used in acoustic trapping to force particles closer together to form clusters. However, for the clusters to become stationary in a moving medium another force plays a crucial role; the lateral primary radiation force.

### The lateral component of the primary radiation force

In essence, what happens in acoustic trapping is that an axial component of the PRF focuses particles towards the nodes in the acoustic fields. As the particles align at the nodal plane, they get close enough to each other for the SRF to provide an attractive force between particles as illustrated in figure 12. The particles have now formed a cluster. The cluster is kept stationary by another element of the PRF denoted the lateral primary radiation force (LPRF). It is believed that the LPRF is formed due to localized actuation of the medium that generates an acoustic field with an intensity gradient that is much steeper in the trapping area than the rest of the channel (figure 15). The theory is that such a localized acoustic field with steep energy gradients provides a force that counteracts the drag force imposed on trapped particles by the fluid flow and retains them at the location of the transducer (figure 14) [47]. The lateral PRF from a standing wave can be written as

Eq 21.
$$F_{L\,PRF} = V\nabla E_{ac}\left(\frac{3(\rho_p - \rho)}{\rho + 2\rho}\cos^2(kx) - \frac{\beta - \beta_p}{\beta}\sin^2(kx)\right)$$

where $E_{ac}$ is the acoustic energy density. Simulations by Hammarström et al. has shown that the pressure drop over microfluidic channel corresponds to the trapping sites observed by microscope [49]

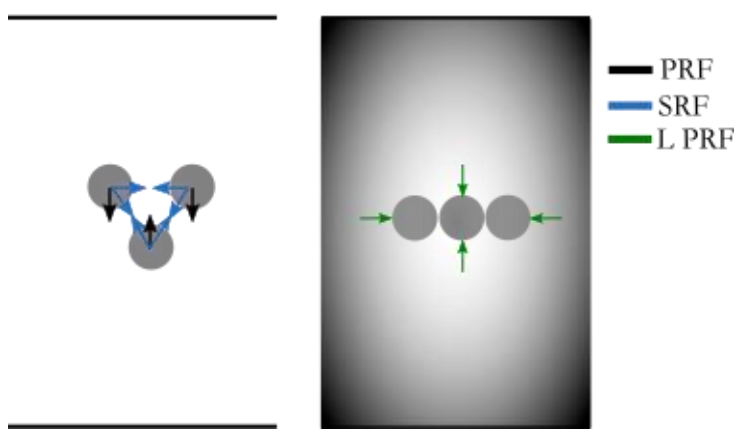


Figure 14. The acoustic field gradient produced the lateral trapping force that contains the particle cluster at the trapping site acting against the acoustic streaming component. Without an applied hydrodynamic force the LPRF will keep the particles levitated. If a flow is applied to the cluster the drag force will be balanced by the LPRF. The gradient in the right image illustrates how the LPRF depends on the energy density of the acoustic fields.

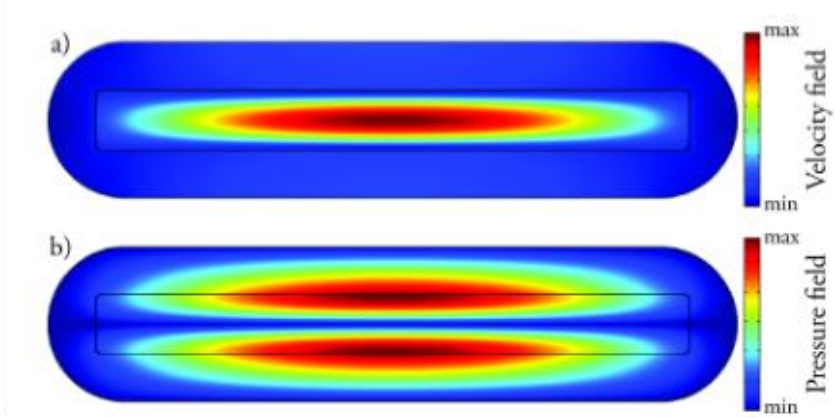


Figure 15 Simulations of the acoustic fields (a -velocity field, b-pressure field) in acoustic trapping in a glass capillary. The pressure node corresponds to the trapping sites in the capillary. At the capillary walls the sound pressure is maximal which repels particle. This figure was obtained from [50].

### Acoustic trapping compared to other microfluidic trapping approaches

Acoustic trapping can handle higher throughput (flowrate) and capacity (amount of trapped sample) than other microfluidic trapping technologies. Greater throughput is desirable for sample preparation and pretreatment in bioanalysis where a large amount of sample fluid needs to be treated to find a measurable amount of analyte. Another strength of acoustic trapping is that samples doesn't have to have beads conjugated to them as in magnetic trapping. The particles polarizability isn't important either as in dielectrophoretic trapping. However as a downside, acoustic trapping has lower resolution than for instance optical trapping where the focus is more on single cells or molecule trapping.

### Seed particles and trapping of small particles

The trapping force determines the highest amount of force from the fluidic drag imposed on the trapping cluster by fluid flow or flow from acoustic streaming that the trap can withstand. Thus, the maximum trapping strength is when the trapping force is equal to the force resulting from the fluidic drag. The lateral primary radiation forces (LPRF), responsible for the trapping force scales with the volume of the particle (eq 21). The fluidic drag scales with the radius of the particle (eq 3 & 19) which means as the particle size is reduced, the trapping force decays at a greater rate than the drag force and the fluidic drag will eventually overcome the trapping force. In acoustic trapping, there will always be a streaming component present that will induce acoustic streaming and thus a drag on the particle. The transition from the streaming dominated regime towards the trapping regime usually occurs at particles of a few micrometers in size. This is a big problem since small particles below or close to the streaming limit like viruses, exosomes and bacteria hold valuable biological information. To solve this issue a technique that allows for capture of particles down

to the nanometer scale using larger micrometer sized seed particles has been developed [47]. In seed particle trapping, the acoustic trap is first pre-loaded with larger particles. These larger particles are able to form stable clusters at the trapping sites that small particles can't. Smaller particles can then be captured by a cluster consisting of a larger pre-formed trap (figure 16). Beyond the size, trapping of particles is also heavily dependent on the concentrations. In the same paper, Hammarström et al. established a relationship between in-trap concentrations of particles and the transitions between streaming and trapping regime. At lower concentrations, the particles are dominated by streaming, i.e. said to be in the streaming regime, while at higher concentrations the interparticle distance is short enough for the SRF to allow formation of a cluster, i.e. the trapping regime.

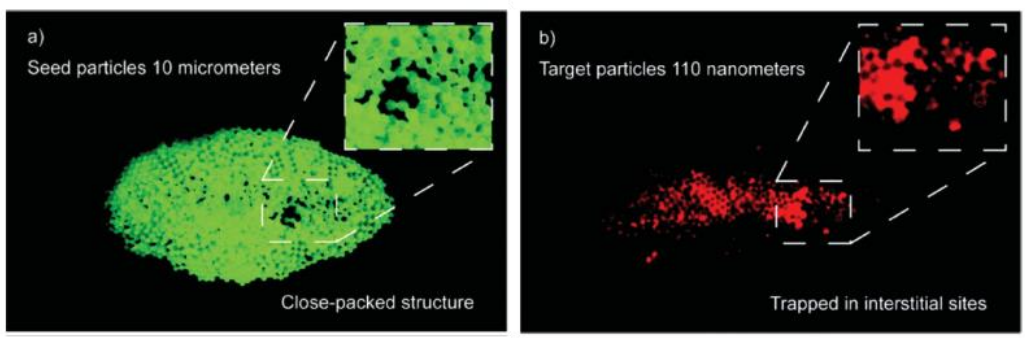


Figure 16 Green fluorescent 10 μm particles used as seed particles to capture red fluorescent 110 nm particles. A) shows the closed packed structure of the seed particles. B) Shows that te the 110 nm particles are trapped between the seed particles in interstitial sites. Obtained from [47].

## Applications of acoustic trapping

In the literature, acoustic trapping has been used in various bioanalytical tasks in order to improve parameters such as resolution, runtime and throughput. Acoustic trapping has been used to prepare the beads for the Luminex system by performing all the incubation steps in an acoustic trap [51]. Antigen coated beads were introduced into the acoustic trap to form clusters and the sample and reagent were then aspirated through the trap for the incubation steps. After incubation, the trap was deactivated and the cluster could be collected and analyzed by the Luminex cytometry system. Acoustic trapping has also been used in conjunction with MALDI-TOF MS (matrix assisted laser desorption/ionization mass spectrometry) to speed up identification of bacteria in blood cultures [52]. The acoustic trap was used to purify bacteria from the background medium with the aid of seed particles. The bacteria was then lysed in the trap and the proteins for the MS analysis were obtained using solid phase extraction (figure 17).

Acoustic trapping is not very suitable for single cell studies, instead it has been widely employed in studies concerning interaction between multiple trapped cells of various kinds. Direct monitoring by video recording of cells levitated in acoustic traps have

been used to determine whether trapped erythrocytes interact and create cell linkages or if they roll past each other and to study the membrane spreading occurring in the trap [53]. Liu et al. aggregated HepG2 hepatocarcinoma cells using acoustic trapping and kept them free from solid substrate as levitated 3D cell cultures for several days [54]. The behavior of the cells in the 3D culture was monitored for up to three weeks and the trapped cells showed similar characteristics as cells prepared by traditional means (figure 18). In another paper a technique for gel-encapsulation of a 3D cell-cluster formed in acoustic traps is demonstrated [55].

Hydrogel-encapsulation could play a preeminent role for the use of cell cultures in direct cell transplantation. Studies have also been performed on mouse embryonic stem cells to investigate if the acoustic pressure and velocity fields affect the gene expression and pluripotency of the stem cells [56]. The study found that gene expression and pluripotency remained unchanged and concluded that the environment in an acoustic trap does not negatively affect cells.

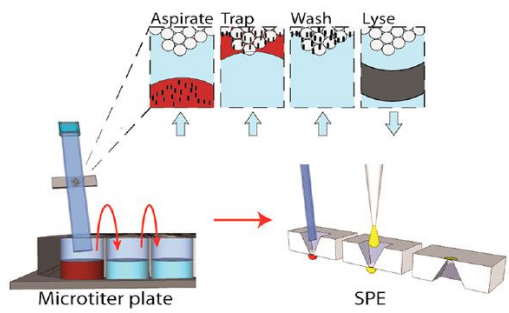


Figure 17. Sample preparation for MALDI-TOF MS using acoustic trapping. The sample and reagents are sequentially flushed through the trapping area. The contents of the trap is lysed and the contents of the cell is extracted using solid phase extraction. Obtained from [52].

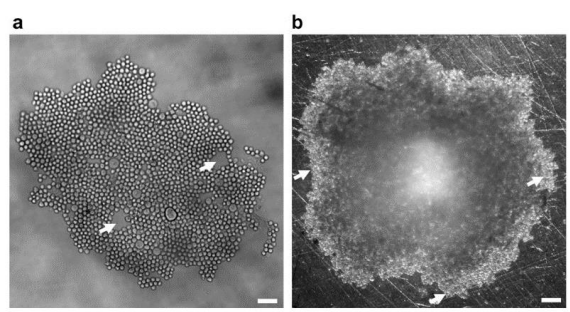


Figure 18 A) A 2-D HepG2 cell cluster levitated in an ultrasound trap. The cells closely aggregate except in few areas (white arrows) where voids can be seen. B) A 3D-HepG2 cell cluster is levitated in an acoustic trap. The cluster has a 3D morphology except in the corners (white arrows) where the cluster collapses into a 2D structure. Obtained from [55].

### Generation of ultrasound - Piezoelectric materials

Piezoelectricity means to derive electricity from pressure and describes a materials ability to induce an electric displacement field that is directly proportional to the applied mechanical stress [57]. The fundamental property of piezoelectric materials is that they can convert mechanical energy in the form of pressure to electrical energy through a process called the direct piezoelectric effect, or the complete opposite i.e. when an electric field is applied to a piezoelectric material it will cause a deformation of the material in a process called the converse piezoelectric effect. Depending on the direction of the electric field, the induced strain of the material may take the form as either expansion or compression. If the electric field is alternating, the strain will give rise to mechanical vibrations in the material with a frequency equal to that of the applied voltage. By applying an AC field over a piezoelectric material one can produce vibrations in air (sound). If this is done at a high enough frequency, ultrasound is produced. Such materials are used in acoustic trapping to build transducers that form the ultrasound that creates the trapping forces.

#### Electrical measurements of piezoelectric materials and ultrasonic transducers

In this thesis, the characteristics and parameters of the trapping transducers were evaluated by electrical impedance/admittance measurements. In general, impedance measurements are desirable for two reasons; they can be used to match the impedance of the driving circuit to that of the trapping transducer and to characterize electrical and mechanical parameters including mechanical losses. From electrical measurement of transducers and piezoelectric materials, one can determine such parameters as the resonance frequency, the mechanical quality factor, the electromechanical coupling coefficient, the loss factor amongst others [58].

At certain frequencies, energy can be easily accumulated in the piezo electric material. These modes are called piezoelectric series resonances. The series resonance mode for a piezoelectric material is characterized by, in theory, infinitesimal electric impedance [59]. In reality, mechanical dampening and losses give non-zero impedance at the series resonance frequency. To emit ultrasonic waves with maximum efficiency, an ultrasonic transducer should be operated at its series resonance frequency [60]. At frequencies other than the series resonance, another form of resonance can occur called parallel resonance or anti-resonance. This resonance is characterized by large impedance [61]. From this point on the series resonance frequency will be referred to as merely the resonance frequency ($f_r$).

At the resonance frequency, equivalent electrical circuits can be used to model the properties of the transducer e.g. the BVD (Butterworth-Van Dyke) model, which is shown in figure 19 [62]. It is common to look at the admittance when analyzing data from impedance measurements.

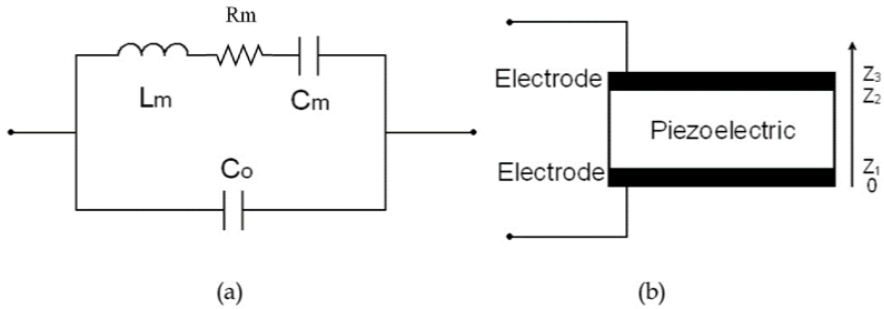


Figure 19. A) The electrical circuit of the BVD model. B) One dimensional representation of a piezoelectric transducer. Obtained from [63].

The admittance is the reciprocal of the impedance and for the BVD model the admittance can be written as,

Eq 22. $$Y_m = \frac{j\omega^2 C_m R_m C_0 - (\omega C_0)(\omega^2 L_m C_m - 1) + \omega C_m}{R_m \omega C_m + j(\omega^2 L_m C_m - 1)}$$

where ω is the angular frequency (ω=2πf) [62]. In figure 20, a typical admittance spectrum for a piezoelectric element is shown. The resonance frequency is the minimum in the impedance spectrum and the maxima in the admittance spectra and vice versa for the anti-resonance. The resonance frequency corresponds to the maximal conductance (G) which is the real part of the admittance. The resonance frequency is described by

Eq 23. $$\omega_r = \frac{1}{\sqrt{L_m C_m}}$$

The mechanical quality factor $Q_m$ describes the shape of the electromechanical resonance spectrum. Usually the motional admittance ($Y_m$), the inverse of the impedance, is plotted around $f_r$ to obtain the $Q_m$. $Q_m$ can be determined in several ways but most commonly the following equation is used

Eq 24. $$Q_m = \frac{\omega}{2\Delta\omega}$$

where $\Delta\omega$ is the bandwidth defined by the FWHM (full width half maximum) at $Y_{max}/2$. Also to note is that the inverse of the mechanical quality factor is equal to the mechanical loss constant for the system [58]. A high value $Q_m$ is represented by a narrow resonance peak while a small $Q_m$ gives a broad resonance peak. A high $Q_m$ value is desired as it corresponds to low degree of mechanical losses in the system. Hammarström et al. developed a method of modifying the shape of the piezoelectric material to stabilize the operation of the piezo [64]. By sawing ridges into the material leaving stripes of piezo referred to as "kerfs", they were able to eliminate spurious

resonances which allows for operation at the correct resonance frequency, which is essential for fabricating transducers with high-$Q_m$ values and for efficient acoustic trapping. In figure 21, the impedance spectrum for a piezo with and without kerfing is shown.

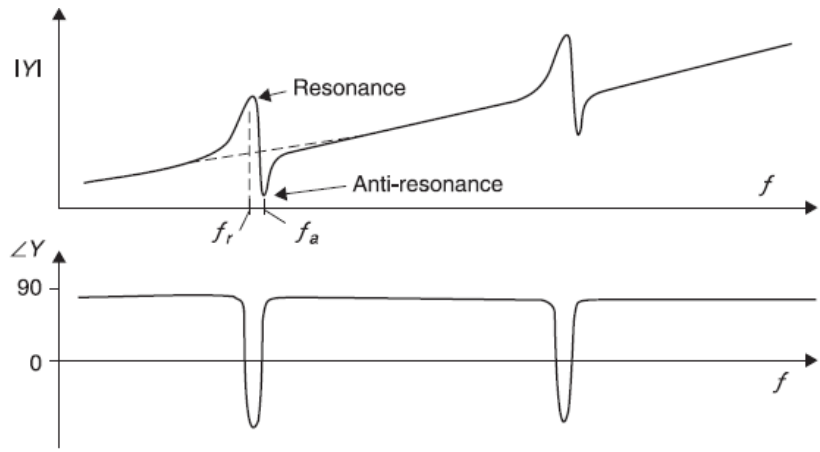


Figure 20. The characteristic admittance of a piezoelectric transducer obtained from impedance analysis. The resonance frequency is at an admittance maximum and the anti-resonance is at an admittance minimum (i.e. the reciprocal of an impedance plot). The flower graph shows the phase transition. Obtained from [58].

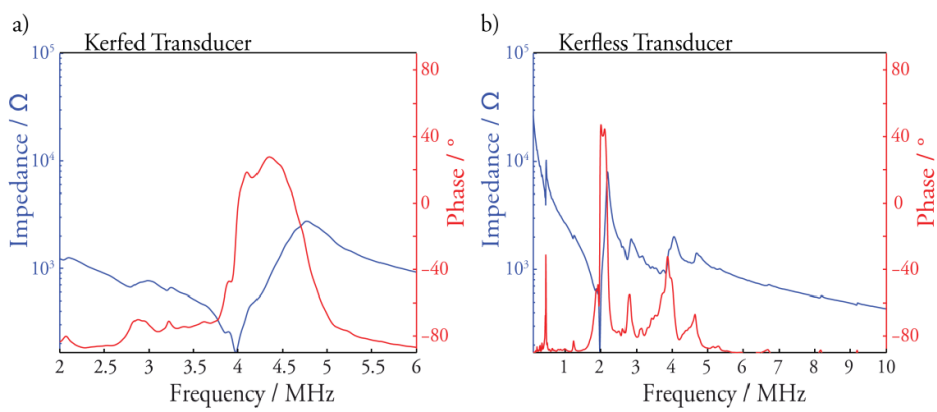


Figure 21. A) Kerfing of the PZT removes spurious nodes and allows for a stable resonance frequency. Blue line is the recorded impedance and red line is the phase. B) Without kerfing there are a lot of other resonances (vibrational modes) present which interferes with device operation. Obtained from [64].

# Materials & Method

## Part I: Improving reproducibility in fabrication of acoustic trapping systems

**Design of acoustic trapping systems**

Earlier in this thesis, the requirements for acoustic trapping were discussed. To achieve acoustic trapping a localized acoustic field is required that generates the lateral trapping force as well as the primary and secondary acoustic forces. A localized, actuation of the trapping medium can be achieved by having a piezoelectric transducer that generates an acoustic field in a defined area of the microchannel where the dimensions of the piezoelectric materials constrains the area of actuation.

In addition to the piezoelectric material, an ultrasonic transducer consists of the backing/dampening layer, the matching layer and the coupling layer [65]. Each layer of materials has distinct acoustic properties to maximize the amount of the acoustic energy generated by the piezoelectric material that produces useful work. The acoustic impedance for the fluid medium is always much lower than the acoustic impedance of the piezoelectric material. A large difference in acoustic impedance leads to high degrees of reflection which means a lot of the acoustic energy will be lost. This is usually addressed using a matching layer which has an impedance that is higher than that of the fluid medium but lower than that of the piezoelectric material. The purpose of the backing layer on the other hand is the complete opposite of the matching layer. The backing layer should provide the maximum difference in acoustic impedance so that the sound is directed towards the desired target. The effect of the backing and matching layer is illustrated in figure 22 below. The coupling layer serves to transmit the acoustic energy between the matching layer and piezoelectric material.

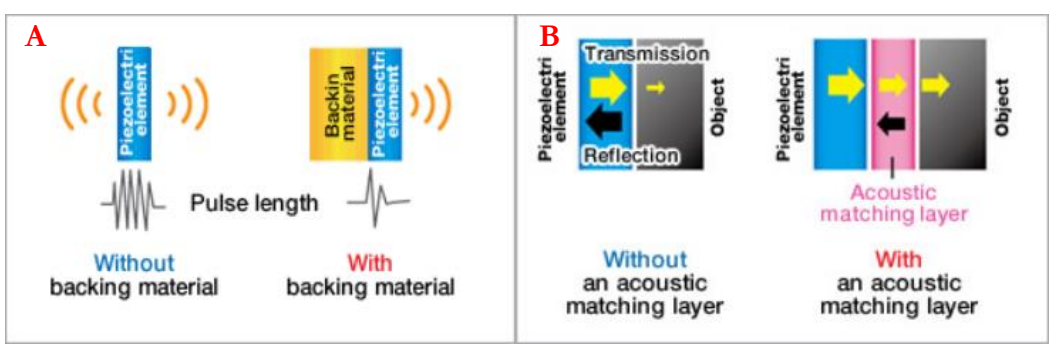


Figure 22. A) This image shows the piezo electric element without and with backing material. B) Image to the left illustrates the transmission with and without the matching layer. The coupling layer has been omitted from these images but it is situated between the matching layer and piezoelectric element to improve transmission of acoustic energy into the matching layer.

In this thesis, the transducer was designed as a layered resonator and is illustrated in figure 23. The piezo was mounted on a PCB (printed circuit board) where the backing layer consisted of air, which is provided by a cut-out in the PCB. The matching layer between the fluid medium and piezo is a glass borosilicate capillary and the coupling layer between the capillary and the piezo was either glycerol or an adhesive. Glycerol is a viscous coupler which means one downside is that the capillary needs to be held in position by a mechanical frame or there is a high risk of misalignment and the capillary can detach from the transducer. Another issue could be the shelf-life of glycerol which is usually 1-2 years. Degradation or exsiccation of the glycerol layer could potentially change device performance over time. An advantage with glycerol coupling is that it provides greater ease of removal and reattachment of the capillary when handling disposable devices for certain biomedical samples.

Another strategy is to use an adhesive as coupling layer that both mechanically and acoustically couples the microchannel to the transducer. Most adhesives used in the electronic industry and for device fabrication, form adhesive bonds by in situ polymerization or polycondensation by either UV or thermal curing [66]. When using an adhesive in fabrication both the material properties of the cured and uncured adhesive are essential. The rheological properties (i.e. viscosity and thixotropic behavior) of the uncured adhesive determines how easily it can be applied in the fabrication process [66]. For acoustic traps, the cured material properties of the adhesive are important since they will determine the acoustic properties of the coupling layer. In this thesis both UV and thermally cured adhesives were investigated for use as a coupling layer and compared with glycerol.

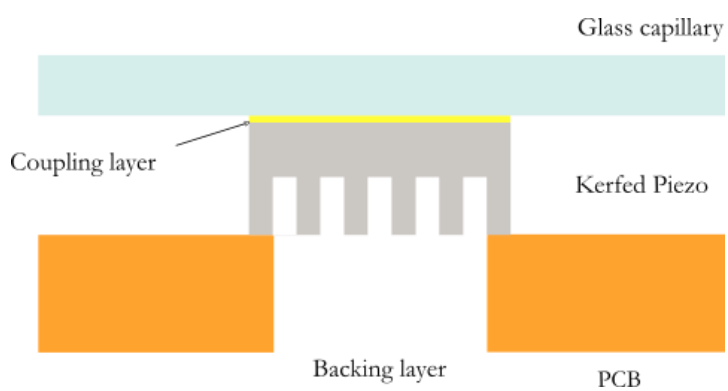


Figure 23. 2D cross-section of a transducer with a capillary for acoustic trapping. The PZT is soldered to a PCB and the glass capillary is bounded to the PZT via a coupling layer. This illustration represents the principal design used for the acoustic trapping transducers in this thesis.

**Fabrication of transducers**

The three major steps in fabrication of acoustic traps are; (1) forming the piezoelectric material into correct dimensions, (2) solder the piezo to the PCB and (3) adhering the microchannel to the piezo on the PCB. These fabrication steps were studied and the characteristics of the devices were analyzed between each fabrication step to identify factors introducing variance between trapping units.

**Forming piezoelectric elements for the transducers**

The fabrication of an ultrasonic transducer starts with manufacturing piezoelectric elements. For the acoustic trapping transducers used in this thesis, the piezoelements were obtained from a PZT wafer (PZT-4/Pz26 Navy I, FerroPerm Piezoceramics, Kvistgaard, Denmark). The formation of individual elements from the wafer starts by kerfing the wafer using a warfer dicing saw (MicroAutomation model 602 M, General Signals Inc, Evansville, IN, USA). The number of kerfs on a single element determines the width of the element. The length of the elements is determined by cutting deeper scores in the wafer perpendicular to the kerfs. After the kerfing procedure, the individual elements for the transducers were formed by placing a scalpel between the kerfs and carefully breaking the PZT so that each element held six kerfs. Six kerfs correspond to a dimension of 3.2 mm long, 0.4 mm thick and 1.15 mm wide piezoelectric element, where the kerfs and ridges are 50 μm and 150 μm wide respectively (figure 24).

The PZT elements were cleaned of debris left by the wafer saw by placing them in a 15 ml Eppendorf tube with ethanol and sonicating them for 20-30 seconds. For identification purposes each piezo was marked with an ID number which allowed for tracking of the units throughout the experiments. The piezos were investigated by impedance analysis using an impedance/gain-phase analyzer with a pin holder (4194A, Hewlett-Packard, Palo Alto, CA, USA). The impedance and phase was recorded for frequencies 2-6 MHz with an applied voltage of 0.5 V.

Figure 24. Back and front of a kerfed piezoelectric element.

### Soldering of transducers

PZT elements that displayed a resonance peak around 4 MHz and had an impedance variation of 18-25 ohm were selected for transducer fabrication. The PZT units were soldered onto PCB (Printed Circuit Board) which holds the required electrical contacts for the transducers. The PCBs were fabricated by isolation milling of copper covered circuit sheets.

### Surface-mount assembly

The soldering technique employed in the fabrication of the transducers is called surface-mount assembly. In surface mount assembly a solder paste is applied to the connectors on the PCB and the components are inserted top-down onto the contact pads. Solder paste was applied to the PCB on the locations for the piezo, external contacts for wave generator/impedance analyzer and silver wire used for contacting the back of the piezo (figure 25). The chip was placed in a solder oven to solder the contacts and piezo to the PCB. A fixture was used to apply a light pressure on the piezo throughout the soldering to avoid changes in position of the piezo (figure 25). The fixture also had a thermocouple which measured the temperature and sent the temperature data to a solder controller. The solder controller regulated the soldering by controlling the heat output of the solder oven (Reflow Controller, BetaLayout, Aarbergen, Germany). The temperature levels set by the solder controller is called a reflow profile. The reflow profile for the solder controller prior to any changes, were made can be seen in figure 26. The profile has 4 important phases. The first step is called pre-heat and is used to ensure even temperature in the oven, to ensure that the flux in the solder flows out and to avoid thermal expansion and cracking of components [67].

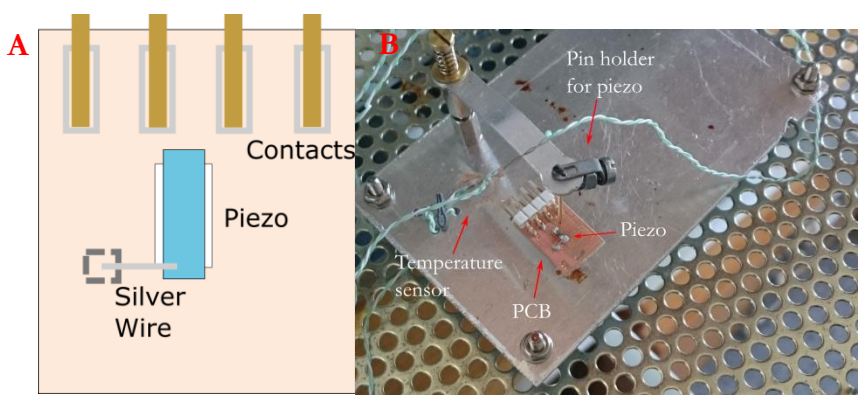


Figure 25. A) A simple illustration of the PCB and the components. The silver wire contacts the back of the piezo and piezo is soldered directly to the PCB. The air backing is situated directly below the piezo. The contacts are for driving the transducer and performing various measurements. B) A fixture was used for making sure the piezo didn't drift during soldering and to record the temperature in the oven during soldering. The holder is resting on the bottom of the tray of the solder oven

The second step is called soak which serve to evaporate and activate the flux and any temperature gradients in the chamber is eliminated. During the reflow and dwell steps the maximum temperature is reached and the components are soldered.

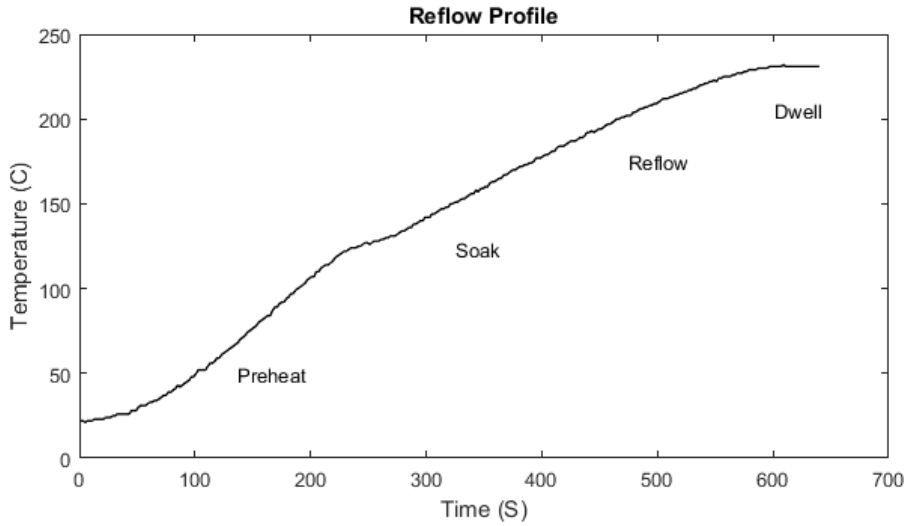


Figure 26. The original reflow profile for the solder oven used in the experiments. The max temperature reached is around 230 °C. Note that this reflow profile was later modified by extending the reflow and dwell times to ensure better soldering.

### Initial solder experiment (Test 1)

The first experiment in soldering of the transducers used a lead free tin based solder paste (NC254, AIMsolder, Montreal, Canada) with a $T_m$ (melting point) of 230 °C. This initial experiment is referred to as test 1. The lead-free solder paste had been used for soldering transducers at the department prior to the start of this project and served as reference point. The purpose with the initial experiment was to document the variations in electrical characteristics produced by the established method of soldering. The transducers were analyzed using impedance measurements and analysis in optical microscope. The impedance and phase was recorded for 0.5 V over the frequency range 2-6 MHz. The $Q_m$, resonance frequency and impedance was used to compare different transducers to each other. The impedance analyzer was controlled using a MatLab script (Matrix laboratory, MathWorks, Natrick, MA, USA) that collected the data output.

### Modifying the solder method (Test 2-4)

The influence of temperature on the variations in electrical characteristics and solder quality was investigated in test 2. Increasing the absolute temperature during soldering is not an option since the piezo can take damage and the soldering oven was already operating at its maximal temperature. Thus soldering using a solder paste with lower

$T_m$ of 183 °C (CR44-SMD, Edsyn, Los Angeles, USA) was used in test 2 to examine if insufficient heat was a problem.

A third test (3) was performed to investigate whether the composition of the solder paste and the reflow profile contributed to bad solders. A new set of transducers were soldered using a modified reflow profile and a fresh flux (NC 297 DX Paste Flux, AIMsolder, Montreal, Canada) was mixed with the solder paste used in test 1. The solder controller was reprogrammed to increase the time spent in the dwell and reflow phase by 40 seconds each. The flux was added to increase wetting and reduce the effects of oxidation. In this experiment the impedance range of the elements prior to soldering were narrowed down to 22-23 Ohm at $f_r$, to test if this would reduce variation of the impedance of the finished transducers. The finished transducers were investigated by optical inspection and impedance analysis as mentioned previously.

Lastly a fourth experiment (4) was conducted using another solder paste (SC BLF 03, Solder Chemistry, Landshut, Germany) to compare to the other results. For this experiment elements with 22-23 Ohm impedance at the resonance frequency were also used. All transducers were analyzed using impedance measurements with 0.5 V with a frequency of 2-6 MHz.

**Coupling of glass capillaries to transducers**

To form reproducible trapping devices, both the fabrication of transducers as well as the attachment of the glass capillary has to be reproducible. The capillary can be coupled using glycerol or adhesive. When using glycerol, the capillary can change position by sliding on the glycerol surface, which induces variation in the performance and electrical characteristics of the device over time. Glycerol coupling was compared with coupling using adhesive. A novel method of attaching the capillary permanently to the transducer using adhesive was developed for this purpose. A PDMS stamp was used to transfer a controlled amount of different types of adhesive materials for coupling of the transducer to the capillary.

Before testing the novel method of coupling capillaries to the transducers, the capillaries themselves were first investigated. If there are large variations in the capillaries themselves, then that will greatly affect how reproducible the coupling will appear.

Measuring variations in the glass capillaries

The glass capillaries (ViroTubes, VitroCom, Mountain Lakes, USA) with a diameter of 0.2 x 2 $mm^2$ are the standard used for acoustic trapping applications at the department. The variation in width and height of the glass capillaries were investigated using an optical microscope by placing the ends of the capillaries facing the microscope's objective. An image was captured and the shape of the capillary was traced in the microscope and image processing software. The dimensions of the

capillary are important as they affect the resonance mode of the trapping device. The data of the capillary measurements were then sent to Department of Physics at DTU where simulation of the resonance for both the measured values and the ones provided by the manufacturer were performed in COMSOL Multiphysics.

### Fabrication of PDMS stamps for adhesive transfer

A master for the PDMS stamp was milled in Polyoxymethylene (POM). The master contains molds for 9 stamps to be manufactured at once. The geometry of the stamp includes of a 2 x 2 cm square base with a 1 x 2.5 mm stamp surface on top of it. A PDMS plaster was obtained by mixing an elastomer base with a curing agent at 10:1 ratio (Sylgard®184 Silicone Elastomer Kit, Dow Corning, Midland, Michigan, USA). The mixture was poured into the master and degassed for 30 min and then placed in a lab stove for 2 hours at 60 ˚C. The stamps were peeled of the master and could be used for transfer of the adhesive.

### Transfer of adhesives to form reproducible acoustic coupling layers

These experiments involve the use of a number of different kinds of adhesives to couple the capillary to the transducer. The adhesives were selected for either their material properties, use in industry or literature or for their ease of use. The selected adhesives were the 353ND (Epoxy Technology Inc., Billerica Ma, USA), NOA86H (Norland Products Inc, Cranbury, NJ, USA) and NOA84 (Norland Products). The 353ND adhesive was provided for free by G A Lindberg ChemTech AB (Mölnlycke, Sweden) and the UV adhesives were purchased from TechOptics Ltd (Tonbridge, Great Britain).

NOA84 and NOA86H are adhesive with low viscosity (40-75 cPs) respective intermediate viscosity (200-300 cPs) and are cured by exposure to UV-light. The NOA adhesives have excellent bond strength to glass and a good bond strength to metal according to the manufacturer. After curing, the shore D hardness is 55 for NOA84 and 75 for NOA86H. Shore D hardness is a measurement scale used for determining how resistant a hard material is to permanent deformation. 353ND is a highly viscous (3000-5000 cPs) two component epoxy that is used in fabrication of medical ultrasound transducers. The manufacturer rates the adhesive as excellent for laminating PZT components and glass. After curing the shore D hardness is 85.

The contact and adhesive transfer process involves first spin coating a thin layer of adhesive on a 22 x 22 mm optical microscope glass slide. Then, adhesive was transferred from the glass slide to a glass capillary using a PDMS stamp. Bonding of the capillary to the transducer was achieved by curing the adhesive in a specially designed fixture to ensure reproducible bonding. The entire process is illustrated in figure 27 and the steps are explained in more detail below. The spin coating step involved dispensing a small amount of adhesive in the middle of a silicon or glass

wafer and running a spin program. The spin program includes a spin-up step (lower rpm) for a short time followed by a spin-off step (higher rpm), usually for a longer time than the spin-up. The actual RPM and time of the spin-up and spin-off steps depend on the viscosity of the adhesives. After running the spin coating program, the glass slide was recovered from the spinner. The adhesive layer on top of the glass slide could now be transferred using a PDMS stamp. To transfer the adhesive, the PDMS was lowered into the adhesive on the glass slide and held for 30 s. The PDMS stamp was then released and pressed against the glass capillary for the same amount of time to transfer the adhesive. The capillary and transducer were aligned in the holder with the adhesive side facing the transducer. The fixture provides a high degree of reproducibility during curing (figure 29). The fixture featured a baseplate, which kept the transducer PCB static and a height adjustable pin that pinched the capillary to the transducer during curing. NOA adhesives were cured by exposure to a UV-light and the epoxy adhesives were cured in a lab stove at 140 ˚C for approximately 1-1.5 hour (353ND) and 80 ˚C for 4 hours (301-2). After curing the pin was raised and the transducer with the capillary could be recovered by simply sliding it out. In figure 28 a finished device can be seen.

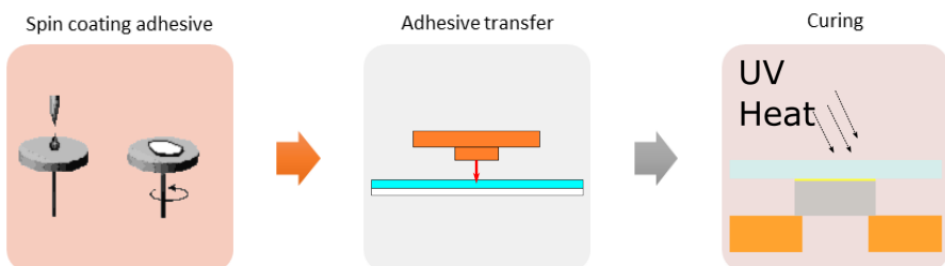


Figure 27. Illustration of the glue coupling/bonding process. The adhesive is spun to a thin layer, transferred using a PDMS stamp and cured. UV or heat is supplied from external sources to cure the adhesive.

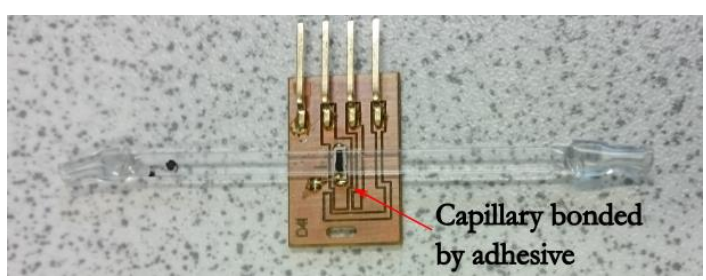


Figure 28. The frame pinching the capillary to the transducer (see figure 30) is not required when the capillary is bonded using adhesives. The adhesives are transparent and the black marks are from a pencil. Some kind of protective cover would be suitable when integrating the trapping device in an analytic system.

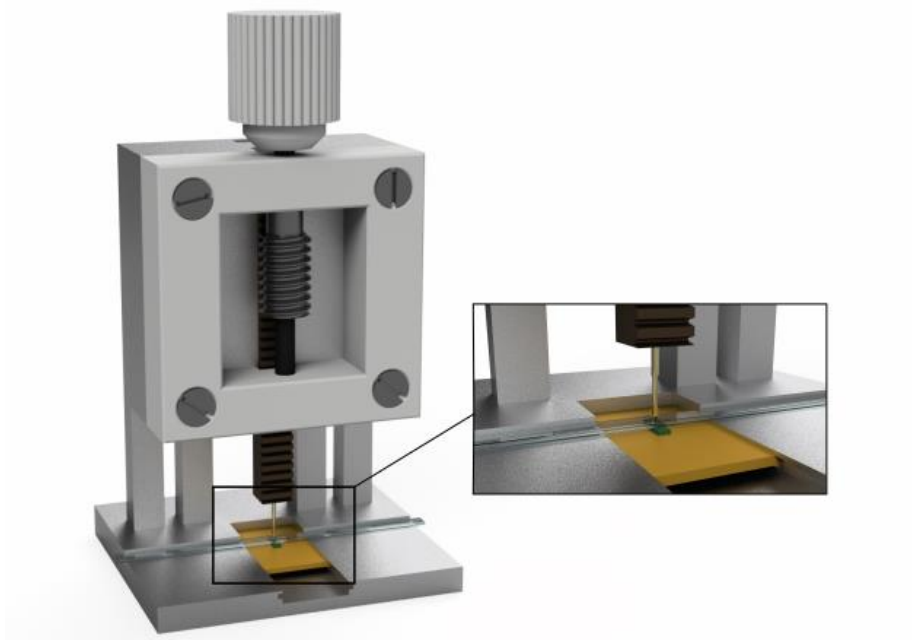

Figure 29. A 3D rendering of the mechanical scaffolding used for reproducible manufacture of trapping devices. A rotating screw handle lowers a pin which presses against the capillary and secures it during curing. The tip of the pin is dampened by spring to control the pressure against the capillary.

### Measuring reproducibility of the adhesive coupling

The reproducibility of the coupling process was tested by measuring the impedance after a capillary had been coupled to a transducer using the method described previously. After impedance had been recorded, the capillaries were detached, cleaned and reattached. This process was repeated for all the adhesives. The combination of capillary and transducer were kept the same within the individual tests. The UV adhesives could be dissolved using acetone, however the epoxy adhesives required the use of the solvent dichloromethane. Repeatedly attaching and removing the capillaries coupled with the adhesives proved to take its toll on the transducers and many broke during course of the experiments.

### Measuring reproducibility of glycerol coupling

A holder for the glycerol measurements was designed and 3D-printed (figure 30). The holder was used to pinch the channel and the transducer against each other since glycerol is a viscous substance. That is not required when the capillary is coupled using an adhesive as the glue will couple the transducer to the capillary both mechanically and acoustically. Each capillary was marked with an ID and paired with a transducer. The capillary was coupled to the transducer by placing drop of glycerol on top of the piezo. A glass capillary was inserted into the holder and placed on top of the glycerol drop. This created a thin layer of glycerol between the capillary and piezo. The glass capillary was filled with water by capillary action or using a syringe

and the impedance was measured. Reproducibility was tested by removing and attaching the capillary multiple times and each time the impedance was measured.

### Trapping in capillaries coupled with adhesive

A quick test was conducted to see if the capillaries coupled with adhesive (NOA86H) would work for trapping. Capacity was measured with and without amplification. 12 µm beads were aspirated into the capillary at a flowrate of 50µl/min and the trap was powered at a frequency selected by the tracking program. The setup and how capacity was measured will be described more thoroughly in the capacity method section.

## Part II: Improving capacity and throughput of acoustic traps

In this part of the thesis devices were manufactured to test if capacity could be increased by using larger capillaries and larger transducers. The larger capillaries have dimensions of 0.2 x 4 $mm^2$ and 0.4 x 4 $mm^2$, and the latter would theoretically make the standing wave oscillate at the first overtone (second harmonics). That means that there would be two nodes in the channel and potentially double the amount of trapping sites. Larger piezoelectric elements might also create a larger acoustic trap that can hold more particles since they cover a larger area of the capillary. The trapping capacity of the new transducers featuring larger channels is compared to standard sized capillaries (0.2 x 2 $mm^2$) with standard sized transducers.

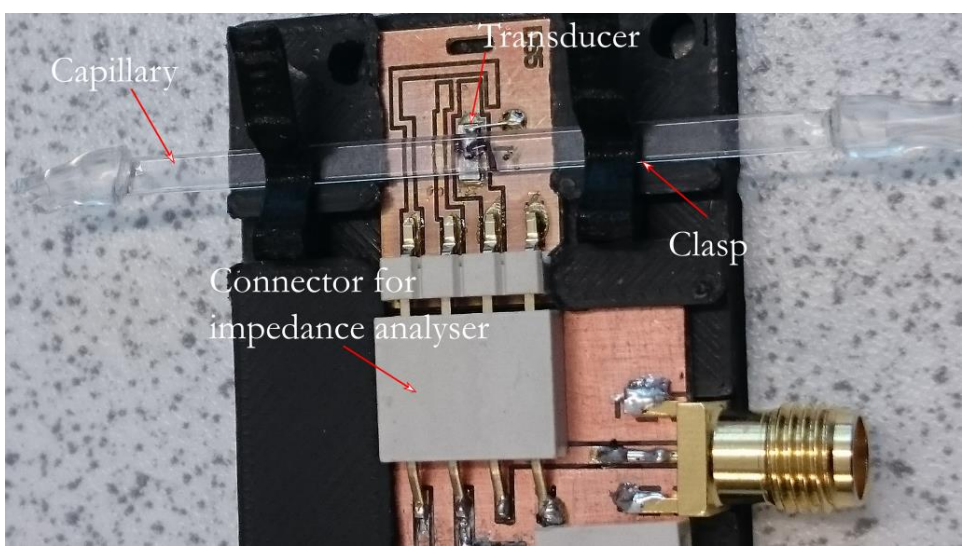


Figure 30. The mechanical frame required to hold the capillary in position when using a viscous coupler like glycerol. The clasps pinch the capillary against the transducer chip. Without the clasps the capillary would simply fall of. The connector ship (bottom part) is used for impedance analysis and attaching a signal generator.

**Fabrication of trapping devices**

A few changes had to be made in the fabrication process to account for the change in the PCB design imposed by the larger capillaries and piezoelectric elements. Each step in the fabrication was investigated with impedance analysis as outlined several times previously in this thesis.

### Forming piezoelectric elements

Three new sizes of piezoelectric elements were formed by cutting and kerfing of a PZT wafer using a wafer dicing saw. The width of the elements were six kerfs (1.15 mm), 9 kerfs (1.75 mm) and 12 kerfs (2.35 mm) respectively. The length of all the elements were 6 mm. After kerfing and cutting, the piezoelectric elements were submerged in ethanol and cleaned by ultra-sonication.

The standard size piezoelectric elements are 6 kerfs (1.15 mm) wide and 3.2 mm long. Thus, being 2.8 mm shorter than the new elements. Increasing the length was required to fit the larger capillaries. Larger area of the piezoelectric element provide transducers with lower impedance. All the transducers can be seen in figure 31 b.

### Transducer fabrication

The PCBs had to be redesigned to account for the larger piezoelectric elements. Two of the contact pads that were designed to be used for temperature monitoring were removed. Two areas were also added to the PCB where spring supports for the capillaries can be soldered on to help protect the capillary and transducer against mechanical stress. The new PCB design is illustrated in figure 31 a. The solder process included applying a solder paste (SC BLF 03) to the areas of the contacts, spring supports, silver wire and piezoelectric element. The fixture presented in Part I in figure 29 was used to keep the piezoelectric element in a static position during soldering.

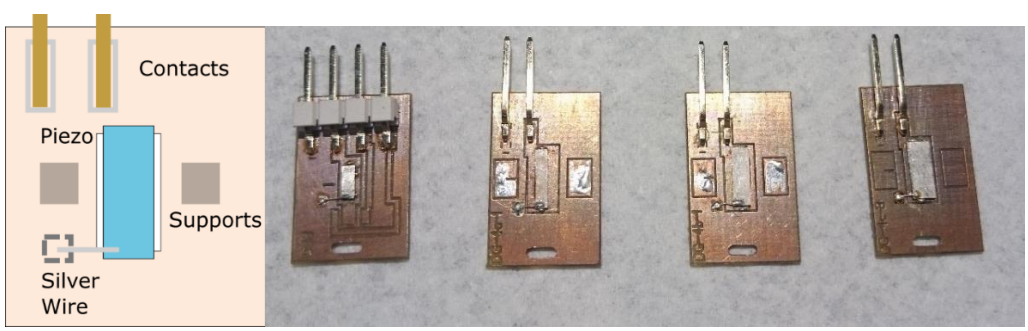


Figure 31. a) The air backing was adjusted to the new seize of the piezoelectric elements. Areas were added where supports for the capillary could be soldered on. Contacts that weren't required were removed, i.e. contacts required for temperature- and other kinds of data collection. b) From the left; the standard transducer followed by the larger six, nine and twelve kerf transducers.

### Coupling of the transducers to the capillaries

Elastic tubing was attached to the inlet and outlet of the capillaries to allow for connection to a syringe pump. Pieces of tubing were shaped to the same form as the capillaries using a heat gun and then glued in place.

The capillaries were not coupled using adhesive during the capacity test. Instead, glycerol was used as a coupler and the capillary was pinched in place using a holder similar to the one displayed in figure 30. The capillaries and transducers could then be easily replaced and the capillaries of different sizes needed to be tested on the same transducer.

### Measuring capacity of the acoustic traps

The experimental setup for testing the capacity is shown in figure 32. The setup consists of a syringe pump (Nemesys, Cetoni, Korbußen, Germany), an optical microscope (SMZ-2T, Nikon, Tokyo, Japan), a camera mounted on the microscope (Inifinity-1, Lumenera, Ottawa, Canada), a signal generator (33220A, Agilent Technologies, Santa Clara CA, USA), a signal amplifier (75A25QA, Amplifier Research, Bothell WA), an oscilloscope (TDS 2002C, Tektronix, Beaverton Oregon, USA) and a holder for the trapping devices. The standard trapping devices were operated using a frequency tracking program which had been developed by Hammerström et al. to optimize and monitor trapping performance. The program identified the best operating frequency by selecting the frequency based upon real-time impedance analysis [64]. Thus, the optimal frequency for trapping was continuously selected. The devices featuring the larger channels were not directly compatible with this program due to their low impedance and thus were operated manually. The manual operation involved sweeping the frequency output from the signal generator and observing the channel, filled with particles, in a microscope. Frequencies where the particles gathered together and formed clusters where further investigated until a stable trap could be formed. The voltage over the transducer was measured using the oscilloscope and if the voltage was to low, the amplifier was used to increase the voltage over the trap to 10 $V_{pp}$.

The capacity was measured by aspirating a solution with 12 μm particles (0.1% v/v tween 20 in DI water) using the syringe pump until the acoustic trap was saturated. Saturation occurred when the trap started losing beads to the drag force of the flow. When a stable trap had been formed, it was flushed with buffer (same as the particles were dispersed in) to clean the channel. The capacity of each trap was measured 3 times. To collect the sample, the signal from the signal generator was turned off and the beads were flushed into a sample Eppendorf tube by ejecting 300 μl of buffer using the syringe pump.

The concentration of beads in the solution in the Eppendorf tubes was determined using a flow cytometer (Accuri C6, BD BioSciences, Franklin Lakes NJ, USA). The flow cytometer counted the amount of particles/volume and from that concentration the total amount of beads in the trap i.e. the capacity was calculated by multiplying the concentration with the ejection volume. The gating of the flow cytometer data is shown in figure 33. The gating was very straight forward since the samples only contained buffer and the 12 µm beads.

The capacity was first measured for the standard 2 x 0.2 $mm^2$ capillary with a standard transducer. The standard channel was then tested on all the new larger transducers. Then, capacity was measured for the 4 x 0.2 $mm^2$ capillary and 4 x 0.4 $mm^2$ on all the new transducers.

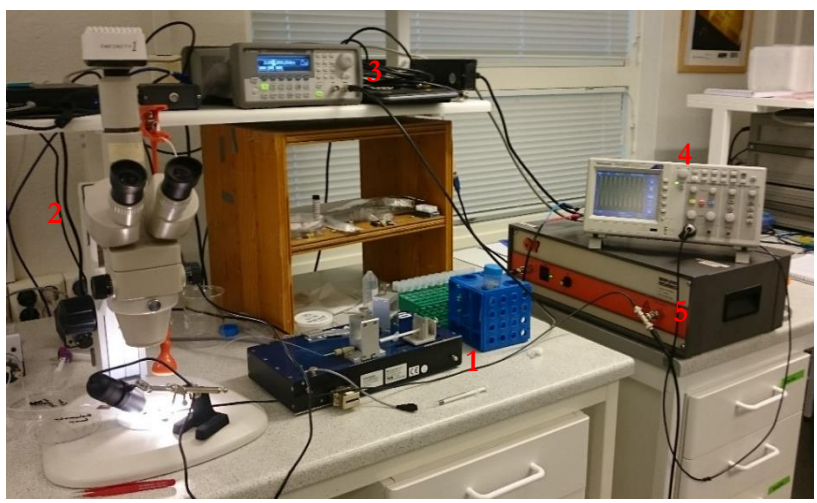


Figure 32. The setup used for measuring the capacity. The pump (1), microscope (2), signal generator (3), oscilloscope (4) and amplifier (5) are visible. The trapping device is positioned under the microscope.

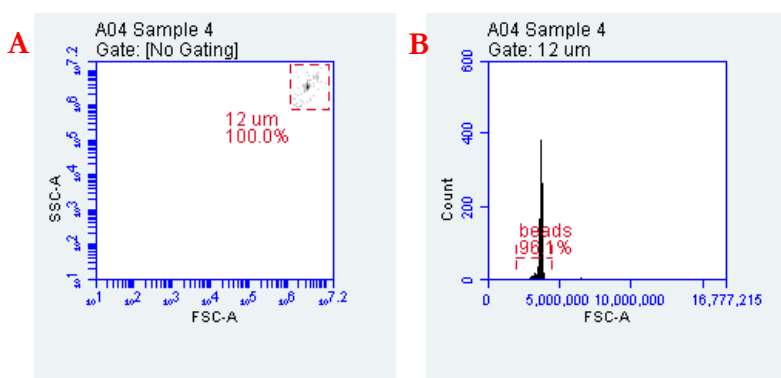


Figure 33. a) The dot-plot of the flow cytometry data. The particles can be seen in the gate named 12 µm. The background interference was eliminated by implementing a threshold. b) The size distribution of the particles inside the 12 µm gate.

# Results

## Part I: Improving reproducibility in fabrication of acoustic trapping systems

**Reproducibility in forming piezoelectric element for the transducers**

Impedance analysis of kerfed piezos showed an average resonance peak at 3.99 MHz. In figure 34, the impedance spectrum of a kerfed piezo is shown for the frequencies 2-6 MHz. In table 1, the average $f_r$, the average impedance at the $f_r$ and the average $Q_m$ of 10 randomly selected piezos is displayed. The $Q_m$ was calculated using a MatLab script (Appendix 1) that converted the impedance to admittance and then extracted $Q_m$. Note that the large standard deviation in $Q_m$ is most likely due to the spring loaded pin holder that held the piezo units in position during impedance analysis. Depending on how the piezo was placed in the pin holder, large variations in mechanical dampening can arise. This manifests itself as a large variation in $Q_m$.

Additional impedance data of each fabrication step can be found in appendix at the end of the report.

Table 1.Impedance analysis data for unmounted piezo. The resonance frequency, impedance at the resonance frequency and $Q_m$ is listed.

| Impedance measurements on kerfed piezos | |
|---|---|
| Average $f_r$ (MHz) | 3.99 ±0.03 |
| Average Impedance at $f_r$ (Ohm) | 26.56±5.40 |
| Average $Q_m$ | 257.25±139 |

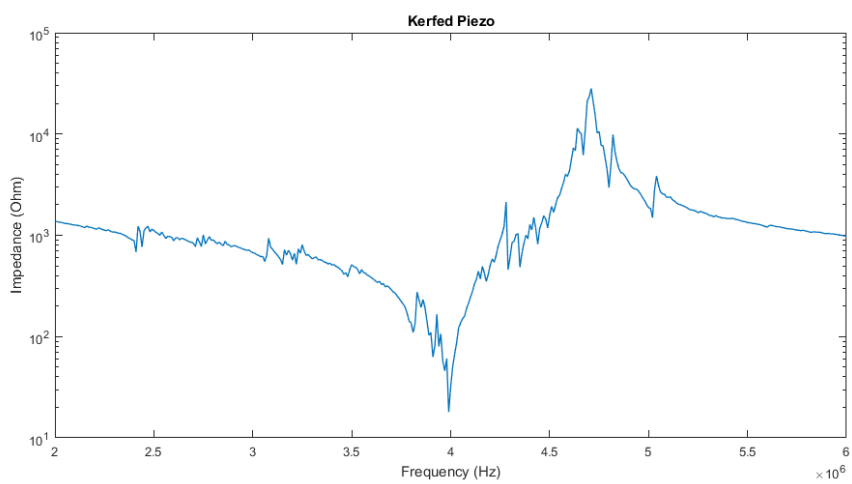


Figure 34. A plot showing impedance analysis of a kerfed piezo with a resonance frequency at 4 MHz and an anti-resonance at 4.71 MHz.

**Reproducibility in soldering of transducers**

Standard method (Test 1)

The initial test of soldering the transducers resulted in low quality solders. The solder paste gave unpredictable results which is not suitable for reproducible soldering. Optical analysis of the solders (figure 35) revealed several issues with the solders. A combination of solder balling, cold joints and non-wetting was identified. Impedance analysis showed, as expected, large variations in electrical characteristics between transducers units (impedance at $f_r$ 44.65±13.40 Ohm and $Q_m$ 128.01±72.92). Note that this variation occurred using elements that had already been selected for their impedance at $f_r$. The results are summarized in table 2.

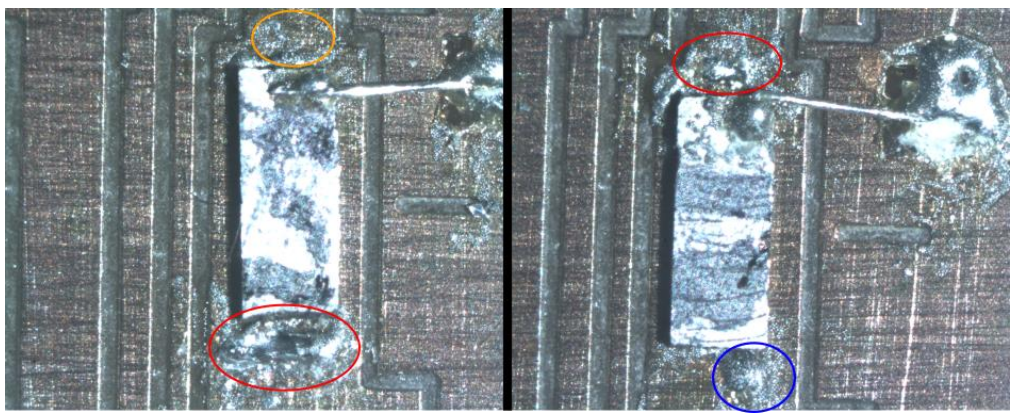

Figure 35. These images were taken in an optical microscope to illustrate the issues with the original soldering method. In the red circled areas, the solder paste hasn't wetted the piezo properly and instead has pulled away from the piezo. In the blue circled area, the solder paste balled up instead of flowing out onto the pad. The orange circle shows that the solder paste granules remains separated after soldering, when they instead should be flowing together creating an even solder.

Modifying the soldering method (test 2-4)

Test 2 (figure 37): Soldering using low temperature solder paste (CR44-SMD) resulted in solders without balling, cold joints or wetting problems. Impedance analysis of these transducers showed a decrease in variation in impedance at $f_r$ and an increase in average impedance (data presented in table 2). The low temperature solder paste was designed for use at 180 ˚C and not 230 ˚C as the solder oven operated at, which had the unwanted effect of the flux evaporating and charring. These tests indicated that one component of the large variations was insufficient heat input during soldering.

Test 3 (figure 38): Clean solders without solder balling, cold joints and wetting problems were produced when the reflow profile was changed and the solder paste used in the first experiment was modified by adding flux. The result of the impedance analysis showed higher average impedance at the resonance frequency than previously

for this solder paste and also lower variation. In this test, piezoelectric elements were carefully selected for their impedance which also brought down the variation.

Test 4 (figure 40): Soldering with the newly purchased solder paste using the new reflow program also resulted in higher average impedance and lower variation in impedance at $f_r$.

All transducers, no matter the fabrication method, showed a decrease of the resonance frequency and an increase in impedance at $f_r$ when the piezo was mounted to the PCB. In figure 36, the impedance spectrum for a transducer and its bare piezo is illustrated. The mounting to a PCB removes instabilities in the piezo by acting as a dampener, but this also increases impedance.

Table 2 The impedance analysis data for the different methods of soldering. The data for the important parameters i.e. resonance frequency, impedance at resonance frequency and $Q_m$-value is reported. The reason for the lower resonance frequency in experiment 3 and 4 is due to the piezo elements used in these experiments had lower starting resonances (same impedance) than previously since they came from a new wafer. The observed drop in frequency after soldering was equivalent to the drop observed in test 1 and 2.

| Solder Paste/Experiment | Average $f_r$ (MHz) | Average Impedance at $f_r$ (Ohm) | Average $Q_m$ |
|---|---|---|---|
| Test 1 (Standard method) | 3.93±0.03 | 44.65±13.40 | 128.01±72.92 |
| Test 2 (Low temperature paste) | 3.92±0.04 | 78.51±8.95 | 74.901±23.42 |
| Test 3 (New soldering program + flux + selection of elements) | 3.85±0.04 | 66.38±2.51 | 88.5±23.88 |
| Test 4 (Change of solder paste) | 3.85±0.03 | 65.55±0.22 | 75.52±28.61 |

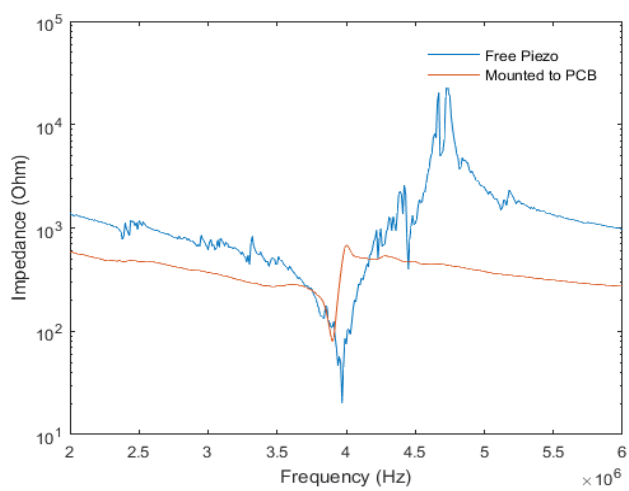


Figure 36. Mounting the piezo to a PCB leads to an increase in impedance at the $f_r$, increased dampening of the piezo and a shift of the $f_r$ towards a lower frequency.

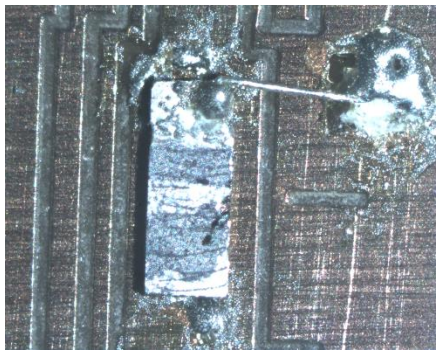

Figure 37. Test 1: Transducer soldered using the standard method. It appears as if the solder paste has problems with wetting the surface properly and that it balls together.

Figure 38. Test 2: Solder paste with low temperature melting point resulted in good solders without the problems visible in figure 42. The flux charred and burned during soldering which is visible as dark areas around the solders.

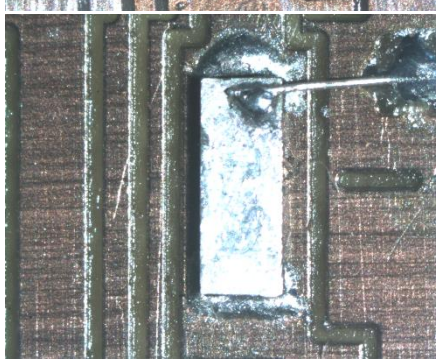

Figure 39. Test 3: Adding flux and modifying the reflow profile of the solder oven resulted in more reproducible soldering using the solder paste NC254. The solder paste wetted the piezo and PCB well which results in higher quality solders than previously (compare figure 42).

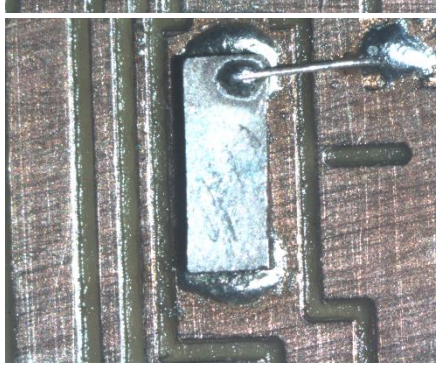

Figure 40. Test 4: Soldering using a newly purchased solder paste with the modified reflow program produced clean solders with minimal variation.

**Reproducibility in coupling of glass capillaries to transducers**

In this section, the investigations of the variations in glass capillaries and the reproducibility of the coupling methods will be presented. The reproducibility of the coupling method using adhesives will be compared to coupling using glycerol.

Variations in glass capillaries

The investigation of the capillaries showed that the thickness and width of the capillary at the ends varied (figure 42). In the 6 capillaries that were measured, the average thickness was 207.46±1.10 µm and the width 2088.97±13.17 µm. The given dimensions of the capillaries in the data sheet is 200 µm by 2000 µm.

The simulations performed at DTU using the measured values and the measurements given by the manufacturer showed that there was a considerable difference in eigenmodes and eigeinfrequencies of the systems depending on the height, width and symmetry of the capillaries [68]. The simulations performed by Ley and Bruus are shown in figure 41. The simulation of a theoretical capillary (a) showed an eigenfrequency of 4.126 MHz and clear pressure node in the capillary. This eigenmode is a bit unstable as there are substantial resonances in the solid glass that might interfere with trapping. Simulations of a real capillary (c), was compared to the perfect capillary in a). Even though there were only small perturbations and irregularities in the real capillary, they showed to impact the resonance mode greatly. For the real capillary, the resonance was highly unstable and there is not a defined pressure node.

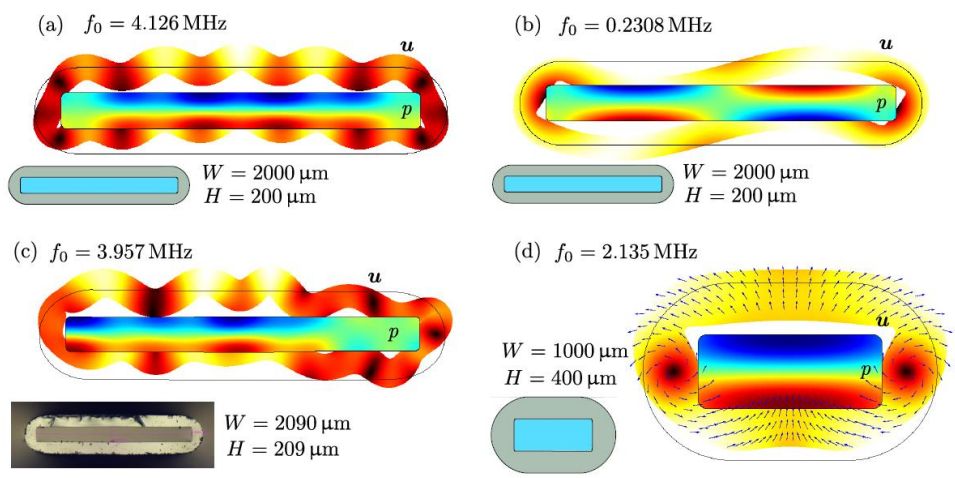


Figure 41. a) The eigenmode for an ideal capillary according to the measurements provided by the manufacturer b) In the simulations it was discovered that at a much lower frequency a resonance mode with two pressure nodes was found c) The dimensions obtained when measuring a real capillary showed in the simulations to give highly unstable resonance modes d) In the simulations, a capillary with the measurements 0.4 x 1 mm$^2$ showed the most stable resonances [68].


Figure 42. The image used by Ley and Bruus for the simulations. The pink lines show how the capillary was measured. Note that the variation of capillary dimensions where the trapping takes place could be higher or lower but these measurements give an indication of the imperfections of the capillaries.

## Reproducibility of Glycerol coupling

When a capillary is coupled to the transducer, the resonance frequency ($f_r$) of the system experiences a shift due to the capillary imposing its resonance frequency on the transducer, as can be seen in figure 43 (green) where the resonance frequency of the transducers is compared with the coupled device. In figure 43, impedance measurements of a system where a capillary has been coupled using glycerol 3 times is also shown. It is difficult to tell from the graph but there is quite a variation in resonance frequency and impedance between glycerol couplings. The first coupling has a $f_r$ of 3.97 MHz and impedance of 133 Ohm, the second coupling have 3.95 MHz and 118.6 MHz and the third 3.93 MHz and 88.57 Ohm. This produces an average resonance frequency of 3.95±0.02 MHz, impedance of 113.39±22.67 and $Q_m$ of 64.13±12.71.

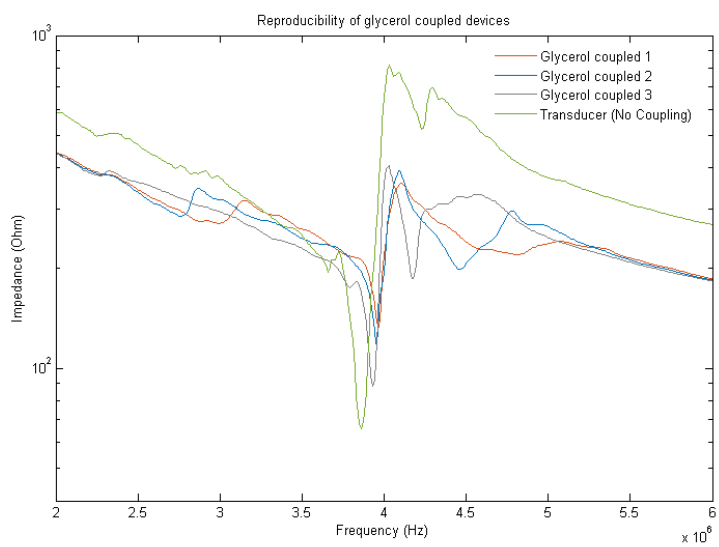


Figure 43. The plot for a single transducer where the capillary has been coupled using glycerol, removed and attached again 3 times. The $f_r$ impedance at the $f_r$ and the peak width vary between attachments. The green trace is of the bare transducer without capillary.

## Reproducibility of adhesive coupling

*NOA86H*

The properties of NOA86H showed to be suitable for the method developed in this thesis to form the coupling layer. The adhesive transferred readily using a PDMS stamp and was cured in a short time using a handheld UV-lamp, which was followed up by a heat treatment. Attaching the capillary to the transducer two times using the adhesive transfer method is shown in figure 44. The first coupling produced an $f_r$ of 3.95 MHz and impedance at $f_r$ of 142.9 Ohm and the second 3.95 MHz and 143.9 Ohm. This led to averages of 3.95±0 MHz, 142.7±0.98 Ohm and $Q_m$ of 99.25±0.35. The impedance measurements can be seen in figure 44.

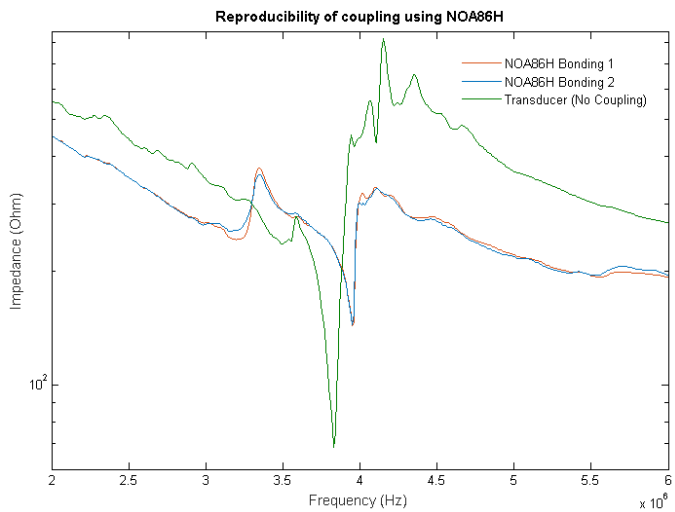


Figure 44. The impedance was recorded for two attachments of the capillary using NOA86H. The green trace is for the naked transducer. The impedance, peak width and resonance frequencies are very similar which indicates a reproducible bonding procedure.

*NOA84*

The NOA84 is a very thin adhesive with low viscosity which allowed for easy transfer using the PDMS stamp. NOA84 showed reproducible bonding when looking at $f_r$ and the impedance at $f_r$. However, the impedance measurements differ around the resonance peak and thus there is a quite large variation in $Q_m$. The first coupling has a resonance of 3.93 MHz and impedance at fr of 160.4 Ohm and the second coupling 3.93 MHz and 155.6 Ohm which produces averages of 3.93±0 MHz, 157.5±3.51 Ohm and 42.52±10.60 $Q_m$. The impedance measurements can be seen in figure 45.

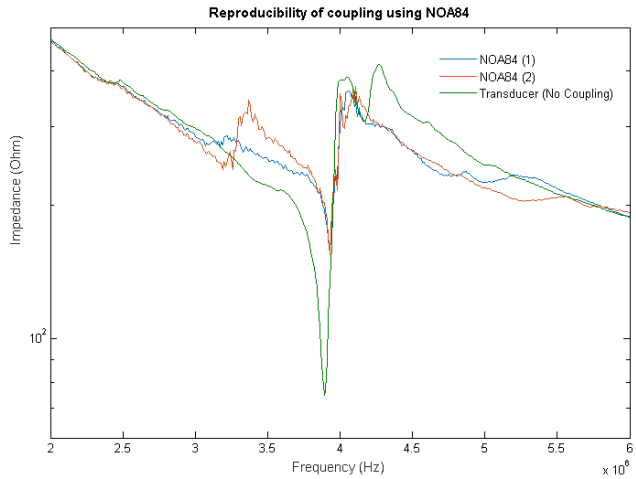


Figure 45. The impedance was recorded for two attachments of the capillary. The impedance at $f_r$, and resonance frequencies are very similar which indicates a reproducible bonding procedure. However the peak width differs a bit which produces a larger variation in $Q_m$

*Reproducibility of 353ND coupling*

The 353ND adhesive was much more viscous than the UV adhesives, having the same viscosity as honey. It was difficult to properly spin coat a glass slide due to the high viscosity and it was also hard to transfer a small amount of adhesive using the PDMS stamp. Large variations in the thickness of the coupling layer was produced with the 353ND which led to lower reproducibility (figure 46). The resonance also lacked the clear peaks that could be seen using the UV-adhesives and had very low $Q_m$. A thicker layer of adhesive should lower the $Q_m$ as the plastic in the coupling layer absorbs acoustic energy. The first coupling produced an $f_r$ of 4.02 MHz and an impedance of 169.7 Ohm and the second coupling produced a $f_r$ of 4.02 MHz and impedance of 201.5 Ohm. This led to averages of 4.02 MHz, 184.6±24.01 Ohm and $Q_m$ of 18±2.82.

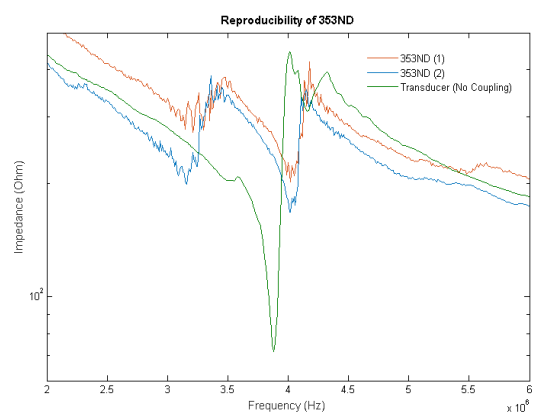


Figure 46. The impedance recording of two attachments of a capillary using 353ND. The traces showed much lower reproducibility and poor performance compared to NOA84 and NOA86H.

*Comparison of NOA86H with NOA84*

Both NOA84 and NOA86H showed high reproducibility and were thus applied to another set of the same transducer and capillary to see if there was any difference in acoustic coupling between the UV-adhesives. Impedance measurements (figure 47) showed that there was no major difference in acoustic coupling. Coupling with NOA86H produced an $f_r$ of 3.95 MHz, impedance of 141 Ohm at $f_r$ and a $Q_m$ of 99. NOA84 gave a $f_r$ of 3.95 MHz, impedance of 138 Ohm at $f_r$ and a $Q_m$ of 99. NOA84 and NOA86H thus seem to have the same acoustic properties, or the material properties of the coupling layer have a minimal effect on the actual coupling as long as a thin enough layer is achieved.

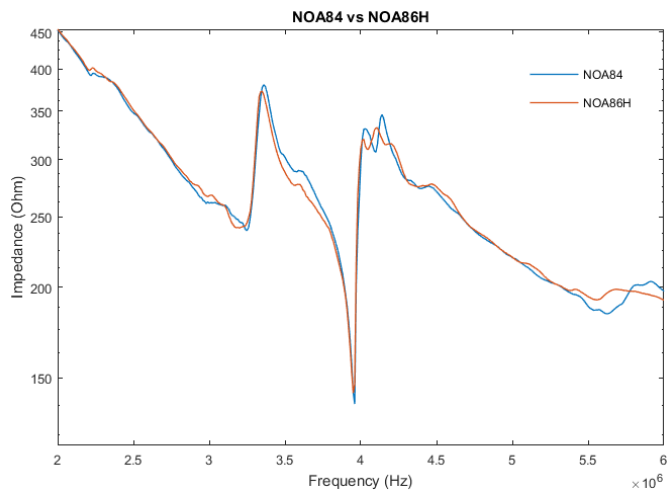


Figure 47. Impedance measurements of the same transducer coupled first with NOA84 and then NOA86H.

## Bond strength of the adhesives

There was no direct experiment conducted to measure the strength of the adhesive that provided the strongest bond between capillary and transducers. However there was still a correlation between the time it took to cure and apply the adhesive to the bond strength. The NOA84 only required UV curing, while the NOA86 required a primary UV curing followed by a heat treatment. The 353ND epoxy adhesive required long curing time at high temperatures. From simply handling the devices and exposing them to manual stress test it could be determined that the NOA84 provided the weakest bond and the bonding would sometimes give out during handling of the device. The NOA86H provided strong bonds that sometimes overcame the solder between piezo and PCB in strength during a manual stress test. The 353ND provided the greatest bond strength and the capillary and transducer would always break before they could be separated.

### Trapping in capillaries coupled with NOA86H adhesive

12 μm polystyrene beads were aspirated into the capillary coupled by adhesives and clusters of particles formed over the piezoelectric element (figure 48). The capacity data of adhesive coupled devices will be presented in the capacity section (Part II) where it will also be compared to glycerol coupled traps.

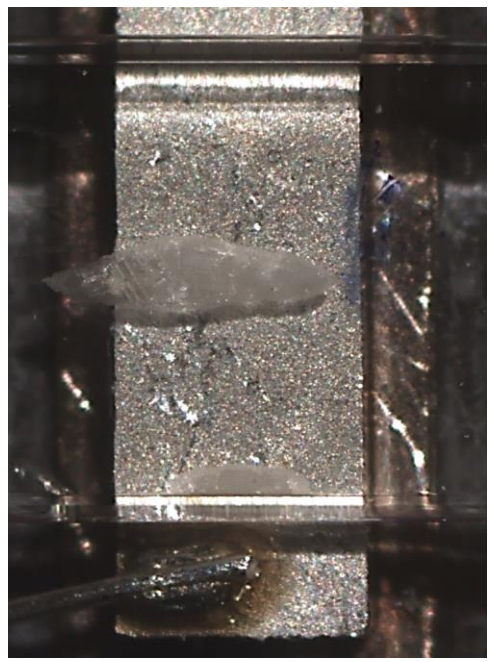

Figure 48. The 12 μm beads were trapped at the center of the piezoelectric element.

# Part II: Improving capacity and throughput of acoustic traps

## Impedance analysis of new transducers

The impedance analysis of the larger transducers devices featuring 6 ($f_r$ 4.03 MHz, impedance at $f_r$ 11.54 Ohm), 9 ($f_r$ 4.12 MHz, impedance at $f_r$ 7.57 Ohm) and 12 ($f_r$ 4.08 MHz, impedance at $f_r$ 7.159 Ohm) kerfs is shown in figure 49. The larger elements have lower impedance than a smaller 6 kerf transducer ($f_r$ 3.84 MHz, impedance at $f_r$ 69.75 Ohm) and the impedance decrease with increasing number of kerfs.

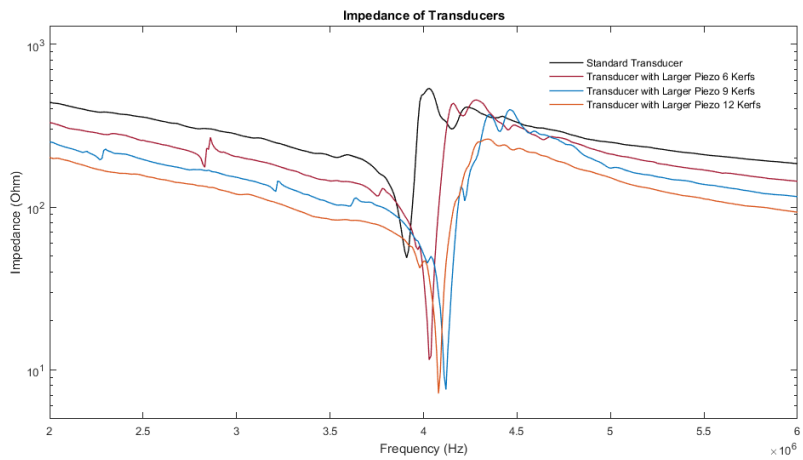


Figure 49. The larger piezoelectric elements produce transducers with much lower impedance. The more kerfs the lower impedance as expected.

## Capacity measurements

The data from all the capacity measurements is summarized in table 3. When using the standard capillary, the capacity increased with the size of the transducer. However this was not the case when using the larger channels. The capacity of trapping using the 0.2 x 4 mm channel did not appear to be related to the size and there was no increase in capacity compared to the standard channel. For the 0.4 mm x 4 mm channel, the capacity was almost four times greater than for the standard channels. The capacity decreased with increasing transducer size. In table 3, the results from all the measurements are displayed. In the standard channel, an acoustic pressure node is formed in the middle of the channel where the beads are trapped as can be seen in figure 50. This also occurs when the standard channel is applied to the larger transducers (figure 51). With the channels of larger dimensions, the pressure node does not seem to form in the center of the channel. Instead there appears to be two nodes, possibly double-nodes, closer to the edges of the channels where particles are trapped (figure 52 & 53). For some combinations these nodes are equally powerful and sometimes one is more powerful than the other.

Table 3. The capacity of the acoustic trap appears to increase with increasing size of the transducer using a standard channel. The capacity of the acoustic traps using the large 0.4 mm x 4 mm decreases with increasing size of the transducer.

| Capacity (Number of beads per µl of sample fluid) | Standard channel | 0.2 mm x 4 mm channel | 0.4 mm x 4 mm channel |
|---|---|---|---|
| Large 6 kerf | 50±2.64 | 53±10.1 | 194±23 |
| Large 9 kerf | 61.67±2.08 | 26.5±2.12 | 173±4.24 |
| Large 12 kerf | 72.33±13.58 | 52.33±13.87 | 167±39.6 |
| Standard channel and transducer | 61.67±2.89 | | |

*Capacity of adhesive coupled traps*

In figure 50 b, trapping in the adhesive coupled device is shown. The device was first tested using only the signal generator outputting around 10 $V_{pp}$ over the piezo. Then the voltage was increased to 20 $V_{pp}$ over the piezo using the amplifier. In table 4 below, the trapping capacity when using 12 µm beads with and without amplification is listed. With amplification the capacity is increased, however it is still half that of the glycerol coupled traps. The shape of the trapping cluster is elongated in the traps coupled with adhesive while it is more focused to one spot for glycerol coupled traps.

Table 4. Table 5. Capacity data from trapping in capillaries trapped with adhesive.

| Mode | Average Capacity (Number of beads per ul of sample fluid) |
|---|---|
| Without amplification | 7.5±3.01 |
| With amplification | 31±3.53 |
| Standard glycerol coupled capillary | 61.67±2.89 |

## Images of traps during capacity measurements

*Standard channel and Reference transducer*

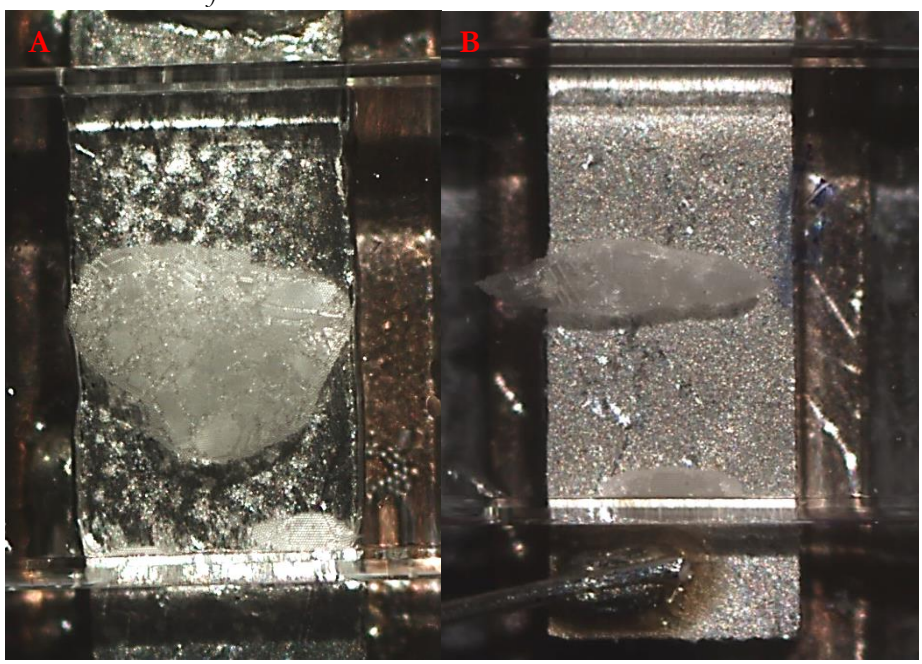


Figure 50. A) Standard channel coupled using glycerol to a standard 6 kerf transducer. A stable cluster is formed at the center of the piezo. B) A standard capillary coupled to a standard 6 kerf transducer using adhesive. There are differences in the shape of the cluster, capacity and stability of the trap between adhesive and glycerol bonded traps. Both are superior using glycerol compared to adhesive.

*Standard channel and new larger transducers*

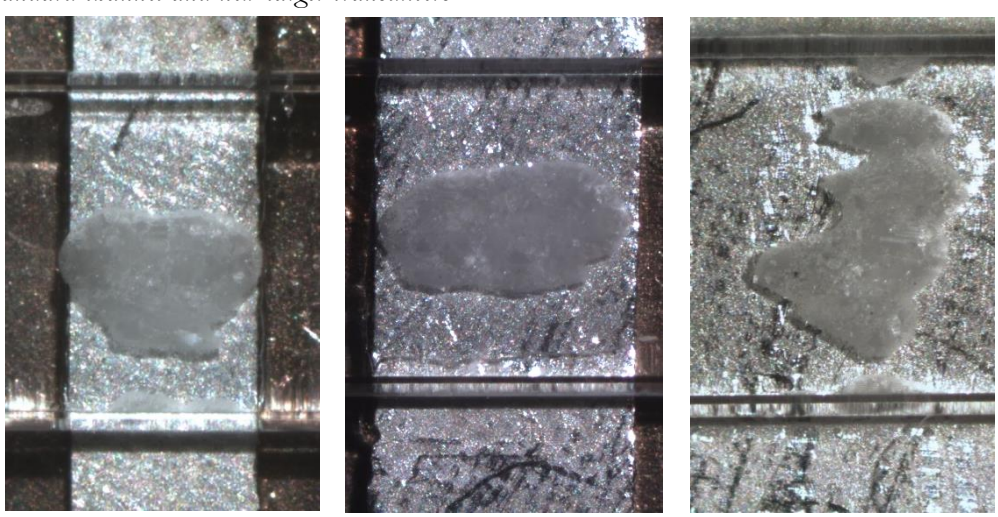

Figure 51. The standard size capillary on the transducers; from left, 6 kerf, 9 kerf and 12 kerf transducers. It appeared as the 12 kerfs had several competing resonances instead of one clear resonance which is why the particles seems to collect at several points on the transducer.

*0.2 x 4 mm² channel and larger transducers*

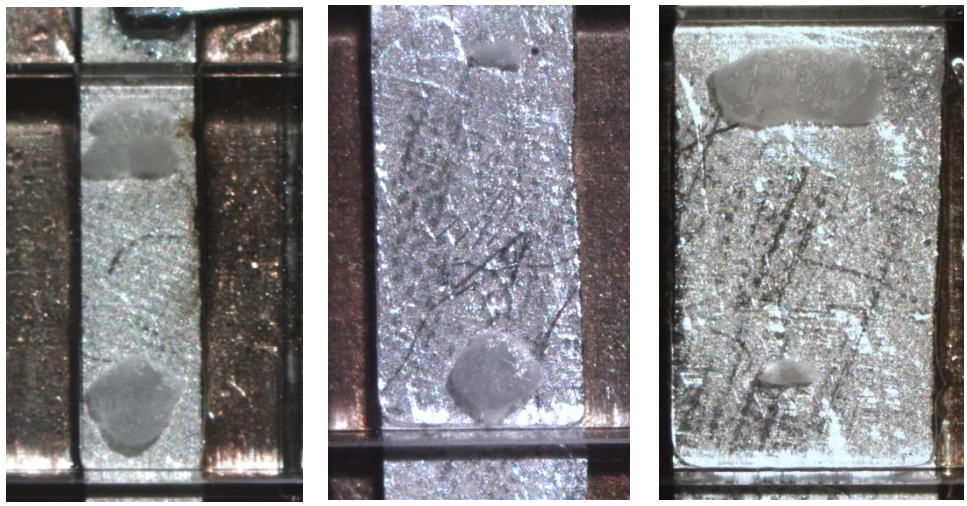

Figure 52. The wider channels combined with the larger transducers produces nodes, one at each side of the channel. The six kerf transducer generated two equally powerful traps while the nine and twelve kerf transducer gave one which was more powerful than the other.

*0.4 x 4 mm² channel and larger transducers*

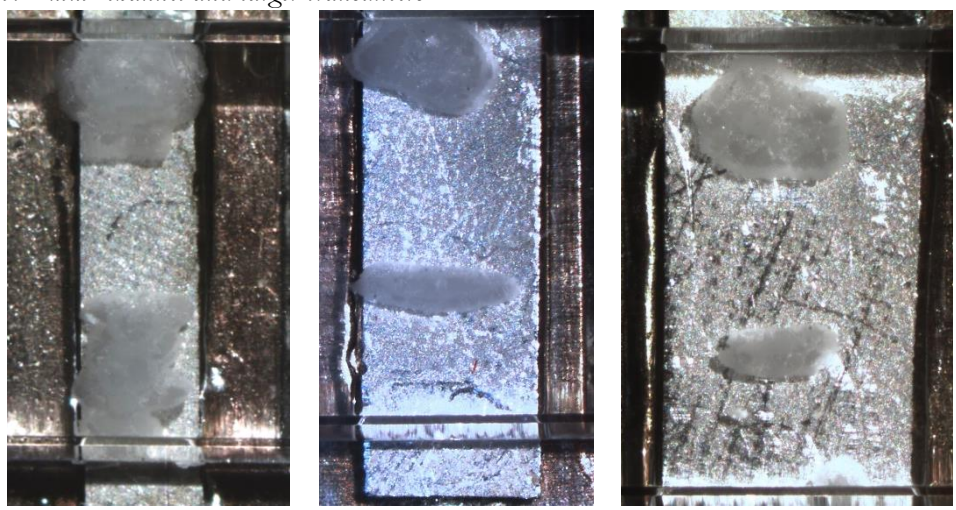

Figure 53. The largest channel produced the highest capacity traps. The six kerf transducer produced the most stable nodes while the 9 and 12 kerf transducers instead produced one stable node and one unstable one.

# Discussion

## Part I: Improvements in reproducibility of acoustic trap fabrication

**Reproducibility in fabrication of piezoelectric elements**

Investigations of the piezoelectric elements after cutting and kerfing procedures showed variations in electrical characteristics that possibly stems from variations in the PZT crystal or damages caused by cutting the wafer, the kerfing procedure or manual cutting steps. Further work could be done to map and document the extent of the variations in electrical characteristics that come from the cutting and kerfing and how much are due to the inherent variation of the PZT material. Optimizing this process would allow for production of transducers with narrow spread in impedance without the need for checking the impedance prior to soldering. This would improve the fabrication process and increase reproducibility.

The resonance frequency around 4 MHz that was measured for the elements is desired since this corresponds with the wavelength required to achieve resonance (standing wave) in the standard size capillaries. Both of these facts corresponds well with the average piezo data presented in table 1.

**Reproducibility in fabrication of transducers**

At the start of this work, the soldering of transducers gave unpredictable results with large variations in the impedance and $Q_m$ at $f_r$. By methodically making changes in the fabrication process, a more reproducible method was developed. The issues identified in the original solder method (test 1) included solder balling, cold joints and wetting problems. Solder balling can arise due to exposure of the solder paste to air (oxidation), exposure to humidity, lack of flux and deficient reflow profile with insufficient dwell times and/or insufficient peak temperature [69]. Cold joints can occur due to insufficient heat input, insufficient amount of flux and surface contamination [67]. Bad solders present a quality and reproducibility issue and can lead to early device failure, change in device performance over time and large difference in electrical characteristics and performance between trapping devices. These issues were solved by improving the solder method.

The parameters that showed to affect the soldering include the selection of piezo elements, the reflow profile and the composition of the solder paste. The tests showed that changing these parameters influenced the variation in impedance seen at $f_r$ and thus the reproducibility in fabrication of transducers. In the end it was shown that transducers could be reproducibly fabricated with an impedance around 65 Ohm at the $f_r$ when the original piezo elements had an impedance around 22-23 Ohm at $f_r$.

The absolute impedance at the resonance frequency increased while the variations in impedance and $Q_m$ decreased as the quality of the solders improved. The current theory is that a better solder constrains the piezo to the PCB more, which results in higher average impedance due to greater dampening of the transducer. A decrease in average $Q_m$ (i.e. an increase in mechanical dampening) for the transducers with better solders supports this theory. A transducer that has deviating impedance at the resonance frequency compared to other transducers could be a sign of a bad solder which could potentially result in early device failure and changes in devices characteristics over time. Since there is a clear correlation between the electrical characteristics and the quality of the solders, this means, impedance analysis of the transducers could be used in quality controls and analysis.

**Reproducibility in coupling of glass capillaries to transducers**

The perks of using glycerol for coupling is that it is easy to attach, remove and adjust the capillary if necessary and it provides good acoustic coupling. On the other hand the disadvantages in using glycerol proved to be low reproducibility and low mechanical robustness. If even a small force was applied to the capillary it would slide on the surface of the piezo and change position, even when clamped against the piezo. A change in position affects the resonance mode of the system and thus the trapping performance.

The simulations carried out at DTU using the capillary measurements showed that the protrusion, irregularities and variations in the glass capillaries influence the resonance mode. This might have impact on the coupling experiments as a change in position of the capillary might result in a change of the resonance mode. If a capillary is not static in location between attachments, then the resonance mode might change as the capillary has variations along its length. That might explain the issues sometimes experienced when using glycerol as a coupler where an acoustic trap will not perform the same after the capillary has been moved. The simulations also show that the shape of the capillaries are far from optimal and that capillaries with the dimensions of 0.4 x 1 $mm^2$ would be far more suitable for trapping (figure 41 d).

A reproducible coupling layer of adhesive was achieved using NOA84 and NOA86H adhesives. The method developed in this thesis can be used to achieve reproducible coupling of the capillary to the transducer. It was observed that for transducers that had very similar electrical characteristics prior to coupling, could look very different from each other after mounting the capillary. Since the coupling process was shown to be reproducible, it leaves the variations in capillaries that can cause these variations following coupling.

As was mentioned in the results, the bond strength of the adhesive differed. The NOA84 provided insufficient bond strength to be applicable, whereas the NOA86H

following heat treatment showed both reproducible bonding and good bond strength. The 353ND epoxy adhesive provided the greatest bond strength but could not be applied in a reproducible manner and had a very cumbersome curing process.

The thermally cured epoxy produced devices with inferior electrical characteristics compared to devices coupled using the UV-adhesives. 353ND have been used successfully by Li et al. as a coupling layer in an acoustic trapping device [70] and the deviating characteristics found in this thesis is most likely due to a thicker layer of adhesive. If a method is developed to achieve equally thin coupling layer using 353ND then similar performance as the UV adhesives might be obtained.

In a study by Hill et al, a model of the layered resonator was created to determine what effect the different layers, i.e. the coupling layer, backing layer and matching layer, had on the electrical characteristics of the resonator [71]. They found that the properties of the adhesive coupling layer only have a relative small effect on electrical characteristics as long as the layer is thin. In their model they could see drastic differences between well bonded devices and poorly bonded devices i.e. thick and thin coupling layers. This corresponds to the results seen in the experiments in this thesis where the thin layers of NOA84 and NOA86 produced very similar results while the thicker coupling layer of 353ND differed.

All the traps coupled using adhesive that were tested trapped beads at a similar degree. The devices coupled with adhesives generally displayed a higher impedance at the resonance peak than glycerol coupled traps (see tables 3-6 in result section). Thus to achieve the same trapping performance as a glycerol coupled trap it could be required to power the adhesive coupled devices at a higher voltage.

## Part II: Improving capacity and throughput of acoustic traps

A number of different combinations of capillaries and transducers were tested and it was possible to more than quadruple the capacity of the acoustic trap compared to the standard trapping setup. Such an increase in capacity can be of interest in various experiments where there is a desire to increase signal strength by increasing trap content, e.g. fluorescence.

For the larger channels, two trapping sites were observed. One of the trapping sites often appeared to be stronger than the other and this might be due to inconsistencies in the dimensions of the capillary, transducer variations or positioning of the capillary. Increasing the width of the channel alone did not produce an increase in the capacity and the 4 mm x 0.2 mm channel produced weak trapping sites with low capacity. On the other hand, increasing both the width and the height of the channel almost quadrupled the capacity for all transducer sizes. Why this is the case is not known at the moment. Perhaps a greater height to width ratio is favorable for trapping. For

instance, the capillary design suggested by DTU for better trapping has a height to width ratio of 0.4/1, the 0.2 mm x 4 mm has a ratio 0f 0.05/1 and 0.4 mm x 4 mm has a ratio of 0.1/1. Perhaps a channel with higher height to width ratio is more advantageous for trapping. This might be related to the acoustic streaming as it is highly dependent on channel dimensions.

The capacity increased linearly with the number of kerfs when using the standard channel. When using devices featuring 12 kerfs it was very difficult to find a stable resonance and it is probably not favorably for trapping to have more than 9 kerfs using a standard channel, even if the capacity is slightly higher.

In theory there should be double nodes in the 0.4 mm x 4 mm channel. It was very hard to study whether the nodes were double or single nodes due the construction of the setup. The setup only allowed for top down observation. To observe the layers, one has to observe the trap from the side. If the trapping sites are double nodes, then the trapping should work as illustrated in figure 55 a. During trapping it appears that the particles did gather in two different planes but it was very hard to capture in an image. A USB microscope was positioned at an angle and an image was taken (figure 55 b). It appears that there are particles in two distinct planes, however it is not clear and would require further studies using a different setup. Another interesting aspect is that if there are 4 nodes that would correlate with the quadrupling of the capacity.

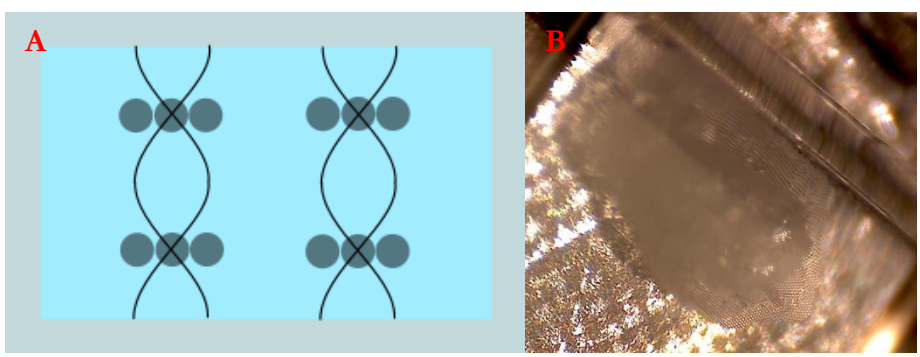


Figure 54. A) There could potentially be two double nodes in the channel. B) USB microscope image at an angle reveals multiple layer of beads.

# Conclusion

Reproducibility and capacity of acoustic trapping are both important factors that were improved upon in this thesis. It was shown that the fabrication of transducers and the coupling of the capillary to a transducer can be made reproducible. Still, these methods contain several parameters that require improvement for transition into full scale production. The method of producing a thin layer of adhesive required for the coupling of the capillary worked well for making one device at the time, but was not suitable for production of multiple devices. There were also issues with getting the adhesive to cover the entire area of the capillary when using the PDMS stamp. These issues can likely be addressed by refining the scaffolding and using an adhesive that can be applied without the use of PDMS stamping.

Variations in the glass capillaries caused two trapping systems that were produced using these reproducible methods to have different characteristics. Thus, capillaries that have more defined dimensions are required to make the process fully reproducible. Development of new capillaries along the lines of those suggested by researchers at DTU would likely improve reproducibility as it would remove unwanted resonances in the glass. Trapping in capillaries coupled using adhesive worked for trapping but there is still development needed for these traps to reach the same capacity as traps coupled using glycerol. From these experiments regarding adhesive coupling, new insights were gained in the fabrication, and advantages and disadvantages with glycerol and adhesive coupling were revealed.

A capacity greater than four times the original was achieved using a combination of larger transducers and capillaries. An even greater increase in capacity can likely be reached by further studies of the transducers and capillary designs. Still, this initial increase in capacity is promising for experiments that require large amounts of analyte to increase the signal to noise ratio. Also, the larger channels allow for greater throughput of sample fluid which can further improve the rate of sample preparation and similar tasks. At this time, it is not known whether having nodes at two places across the channel is an advantage or a disadvantage. For instance, you could use the different trapping sites as control groups towards each other or perhaps by using laminar flows in order to expose the two sites to different reagents.

# References


1.Ashkin, A., et al., *Observation of a single-beam gradient force optical trap for dielectric particles.* Optics letters, 1986. **11**(5): p. 288-290.

2.Rayleigh, L., *XXXIV. On the pressure of vibrations.* The London, Edinburgh, and Dublin Philosophical Magazine and Journal of Science, 1902. **3**(15): p. 338-346.

3.Sarvazyan, A.P., O.V. Rudenko, and W.L. Nyborg, *Biomedical applications of radiation force of ultrasound: historical roots and physical basis.* Ultrasound in medicine & biology, 2010. **36**(9): p. 1379-1394.

4.Evander, M., et al., *Noninvasive acoustic cell trapping in a microfluidic perfusion system for online bioassays.* Analytical chemistry, 2007. **79**(7): p. 2984-2991.

5.Mariella Jr, R., *Sample preparation: the weak link in microfluidics-based biodetection.* Biomedical microdevices, 2008. **10**(6): p. 777-784.

6.Kole, P.L., et al., *Recent advances in sample preparation techniques for effective bioanalytical methods.* Biomedical Chromatography, 2011. **25**(1-2): p. 199-217.

7.McDowall, R., *Sample preparation for biomedical analysis.* Journal of Chromatography B: Biomedical Sciences and Applications, 1989. **492**: p. 3-58.

8.Evander, M. and J. Nilsson, *Acoustofluidics 20: applications in acoustic trapping.* Lab on a chip, 2012. **12**(22): p. 4667-4676.

9.Whitesides, G.M., *The origins and the future of microfluidics.* Nature, 2006. **442**(7101): p. 368-373.

10.Li, D., *Encyclopedia of microfluidics and nanofluidics*. 2008: Springer Science & Business Media.

11.Squires, T.M. and S.R. Quake, *Microfluidics: Fluid physics at the nanoliter scale.* Reviews of modern physics, 2005. **77**(3): p. 977.

12.Beebe, D.J., G.A. Mensing, and G.M. Walker, *Physics and applications of microfluidics in biology.* Annual review of biomedical engineering, 2002. **4**(1): p. 261-286.

13.Van Dyke, M. and S. Widnall, *An album of fluid motion.* Journal of Applied Mechanics, 1983. **50**: p. 475.

14.Amini, H., W. Lee, and D. Di Carlo, *Inertial microfluidic physics.* Lab on a Chip, 2014. **14**(15): p. 2739-2761.

15.Wong, S.H., M.C. Ward, and C.W. Wharton, *Micro T-mixer as a rapid mixing micromixer.* Sensors and Actuators B: Chemical, 2004. **100**(3): p. 359-379.

16.Stroock, A.D., et al., *Chaotic mixer for microchannels.* Science, 2002. **295**(5555): p. 647-651.

17.Bayraktar, T. and S.B. Pidugu, *Characterization of liquid flows in microfluidic systems.* International Journal of Heat and Mass Transfer, 2006. **49**(5): p. 815-824.

18.Stone, H.A. and S. Kim, *Microfluidics: basic issues, applications, and challenges.* AIChE Journal, 2001. **47**(6): p. 1250-1254.

19.Oh, K.W., et al., *Design of pressure-driven microfluidic networks using electric circuit analogy.* Lab on a Chip, 2012. **12**(3): p. 515-545.

20.Xia, Y. and G.M. Whitesides, *Soft lithography.* Annual review of materials science, 1998. **28**(1): p. 153-184.
21.Anderson, J.R., et al., *Fabrication of microfluidic systems in poly (dimethylsiloxane).* Electrophoresis, 2000. **21**(1): p. 27-40.
22.McDonald, J.C. and G.M. Whitesides, *Poly (dimethylsiloxane) as a material for fabricating microfluidic devices.* Accounts of chemical research, 2002. **35**(7): p. 491-499.
23.Helene, L., et al., *Microscale multiple biomolecules printing in one step using a PDMS macrostamp.* Microelectronic Engineering, 2009. **86**(4): p. 1428-1430.
24.Kaufmann, T. and B.J. Ravoo, *Stamps, inks and substrates: polymers in microcontact printing.* Polymer Chemistry, 2010. **1**(4): p. 371-387.
25.Whitesides, G.M., et al., *Soft lithography in biology and biochemistry.* Annual review of biomedical engineering, 2001. **3**(1): p. 335-373.
26.Johann, R.M., *Cell trapping in microfluidic chips.* Analytical and bioanalytical chemistry, 2006. **385**(3): p. 408-412.
27.Chen, J., J. Li, and Y. Sun, *Microfluidic approaches for cancer cell detection, characterization, and separation.* Lab on a Chip, 2012. **12**(10): p. 1753-1767.
28.Antia, M., T. Herricks, and P.K. Rathod, *Microfluidic approaches to malaria pathogenesis.* Cellular microbiology, 2008. **10**(10): p. 1968-1974.
29.Nilsson, J., et al., *Review of cell and particle trapping in microfluidic systems.* Analytica chimica acta, 2009. **649**(2): p. 141-157.
30.Karimi, A., S. Yazdi, and A. Ardekani, *Hydrodynamic mechanisms of cell and particle trapping in microfluidics.* Biomicrofluidics, 2013. **7**(2): p. 021501.
31.Hur, S.C., A.J. Mach, and D. Di Carlo, *High-throughput size-based rare cell enrichment using microscale vortices.* Biomicrofluidics, 2011. **5**(2): p. 022206.
32.Di Carlo, D., N. Aghdam, and L.P. Lee, *Single-cell enzyme concentrations, kinetics, and inhibition analysis using high-density hydrodynamic cell isolation arrays.* Analytical chemistry, 2006. **78**(14): p. 4925-4930.
33.Yang, L., *A review of multifunctions of dielectrophoresis in biosensors and biochips for bacteria detection.* Analytical Letters, 2012. **45**(2-3): p. 187-201.
34.Voldman, J., et al., *Design and analysis of extruded quadrupolar dielectrophoretic traps.* Journal of electrostatics, 2003. **57**(1): p. 69-90.
35.Neuman, K.C. and A. Nagy, *Single-molecule force spectroscopy: optical tweezers, magnetic tweezers and atomic force microscopy.* Nature methods, 2008. **5**(6): p. 491.
36.Neuman, K.C. and S.M. Block, *Optical trapping.* Review of scientific instruments, 2004. **75**(9): p. 2787-2809.
37.Svoboda, K., et al., *Direct observation of kinesin stepping by optical trapping interferometry.* Nature, 1993. **365**(6448): p. 721-727.
38.Pilát, Z., et al., *Optical trapping of microalgae at 735–1064nm: Photodamage assessment.* Journal of Photochemistry and Photobiology B: Biology, 2013. **121**: p. 27-31.
39.Kinsler, L.E., et al., *Fundamentals of acoustics.* Fundamentals of Acoustics, 4th Edition, by Lawrence E. Kinsler, Austin R. Frey, Alan B. Coppens, James V.

Sanders, pp. 560. ISBN 0-471-84789-5. Wiley-VCH, December 1999., 1999: p. 560.
40.Gor'Kov, L. *On the forces acting on a small particle in an acoustical field in an ideal fluid*. in *Soviet Physics Doklady*. 1962.
41.Manneberg, O., *Multidimensional ultrasonic standing wave manipulation in microfluidic chips.* 2009.
42.Bjerknes, V., *Die Kraftfelder*. 1909: F. Vieweg.
43.Gröschl, M., *Ultrasonic separation of suspended particles-Part I: Fundamentals.* Acta Acustica united with Acustica, 1998. **84**(3): p. 432-447.
44.Nyborg, W.L., *Acoustic streaming due to attenuated plane waves.* The journal of the acoustical society of America, 1953. **25**(1): p. 68-75.
45.Sadhal, S., *Acoustofluidics 13: Analysis of acoustic streaming by perturbation methods.* Lab on a Chip, 2012. **12**(13): p. 2292-2300.
46.Bruus, H., *Acoustofluidics 10: scaling laws in acoustophoresis.* Lab on a Chip, 2012. **12**(9): p. 1578-1586.
47.Hammarström, B., T. Laurell, and J. Nilsson, *Seed particle-enabled acoustic trapping of bacteria and nanoparticles in continuous flow systems.* Lab on a Chip, 2012. **12**(21): p. 4296-4304.
48.Kundt, A. and O. Lehmann, *Ueber longitudinale Schwingungen und Klangfiguren in cylindrischen Flüssigkeitssäulen.* Annalen der Physik, 1874. **229**(9): p. 1-12.
49.Hammarström, B., et al., *Non-contact acoustic cell trapping in disposable glass capillaries.* Lab on a Chip, 2010. **10**(17): p. 2251-2257.
50.Hammarström, B., *Acoustic Trapping in Biomedical Research*. 2014, Lund University.
51.Tenje, M., et al., *Acoustic trapping as a generic non-contact incubation site for multiplex bead-based assays.* Analytica chimica acta, 2015. **853**: p. 682-688.
52.Hammarström, B.r., et al., *Acoustic trapping for bacteria identification in positive blood cultures with MALDI-TOF MS.* Analytical chemistry, 2014. **86**(21): p. 10560-10567.
53.Coakley, W., et al., *Cell–cell contact and membrane spreading in an ultrasound trap.* Colloids and Surfaces B: Biointerfaces, 2004. **34**(4): p. 221-230.
54.Liu, J., et al., *Functional three-dimensional HepG2 aggregate cultures generated from an ultrasound trap: Comparison with HepG2 spheroids.* Journal of cellular biochemistry, 2007. **102**(5): p. 1180-1189.
55.Bazou, D., et al., *Long-term viability and proliferation of alginate-encapsulated 3-D HepG2 aggregates formed in an ultrasound trap.* Toxicology in Vitro, 2008. **22**(5): p. 1321-1331.
56.Bazou, D., et al., *Gene expression analysis of mouse embryonic stem cells following levitation in an ultrasound standing wave trap.* Ultrasound in medicine & biology, 2011. **37**(2): p. 321-330.
57.Safari, A. and E.K. Akdogan, *Piezoelectric and acoustic materials for transducer applications*. 2008: Springer Science & Business Media.
58.Nakamura, K., *Electrical evaluation of piezoelectric transducers.* Ultrasonic Transducers: Materials and Design for Sensors, Actuators and Medical Applications, 2012: p. 264.

59.Uchino, K., *Introduction to piezoelectric actuators and transducers*. 2003, DTIC Document.
60.Getman, I. and S. Lopatin. *Matching of series and parallel resonance frequencies for ultrasonic piezoelectric transducers*. in *Applications of Ferroelectrics, 2000. ISAF 2000. Proceedings of the 2000 12th IEEE International Symposium on*. 2000. IEEE.
61.Stutts, D. *A simple example of the relationship between electromechanical coupling and measured impedance*. 1995 [cited 2016 20/4]; Available from: http://web.mst.edu/~piezo/MotorAnalysis/Impedancemodel/Imped-Mo.html.
62.Huang, H. and D. Paramo, *Broadband electrical impedance matching for piezoelectric ultrasound transducers.* Ultrasonics, Ferroelectrics, and Frequency Control, IEEE Transactions on, 2011. **58**(12): p. 2699-2707.
63.Chatras, M., et al., *Modeling and design of BAW resonators and filters for integration in a UMTS transmitter.* Modeling and Measurement Methods for Acoustic Waves and for Acoustic Microdevices, 2013: p. 323-354.
64.Hammarström, B., et al., *Frequency tracking in acoustic trapping for improved performance stability and system surveillance.* Lab on a Chip, 2014. **14**(5): p. 1005-1013.
65.Cannata, J.M., et al., *Design of efficient, broadband single-element (20-80 MHz) ultrasonic transducers for medical imaging applications.* Ultrasonics, Ferroelectrics, and Frequency Control, IEEE Transactions on, 2003. **50**(11): p. 1548-1557.
66.Rabilloud, G., *Adhesives in electronics.* Handbook of Adhesives and Sealants, 2005. **1**: p. 349-483.
67.Lee, N.-C., *Reflow soldering processes and troubleshooting: SMT, BGA, CSP, and flip chip technologies*. 2002: Newnes.
68.Ley, M. and H. Bruus, *Design considerations of acoustic modes in glass capillaries used in acoustic trapping devices.* Acoustofluidics 2016, 2016.
69.Arra, M., et al., *Solder balling of lead-free solder pastes.* Journal of electronic materials, 2002. **31**(11): p. 1130-1138.
70.Li, S., et al., *Application of an acoustofluidic perfusion bioreactor for cartilage tissue engineering.* Lab on a Chip, 2014. **14**(23): p. 4475-4485.
71.Hill, M., Y. Shen, and J.J. Hawkes, *Modelling of layered resonators for ultrasonic separation.* Ultrasonics, 2002. **40**(1): p. 385-392.

# Appendix:

Script for converting impedance to conductance and extracting $Q_m$ was supplied by the supervisor. P is the phase, Z is the impedance and F is the frequency.

```
P=P*pi/180;
Z=Z.*exp(j*P);

Y=1./Z;
G=real(Y);
B=imag(Y);

[Gmax,i]=max(G);
Fmax=F(i);
FWHM=Gmax/2;

F_index=find(G>FWHM);
Flow=F(F_index(1));
Fhigh=F(F_index(end));

Q=Fmax/(Fhigh-Flow);

Q
Fmax/1e6

%%
hFig = figure(5);
set(hFig, 'Position', [100 100 1000 800])
plot(F,G)
hold on
plot(Fmax,Gmax,'ro')
plot(F(F_index(1)),G(F_index(1)),'ro')
plot(F(F_index(end)),G(F_index(end)),'ro')

clear i F_index b
```

Impedance data

Forming piezoelectric elements

The image shows a number of randomly selected kerfed piezoelectric elements.

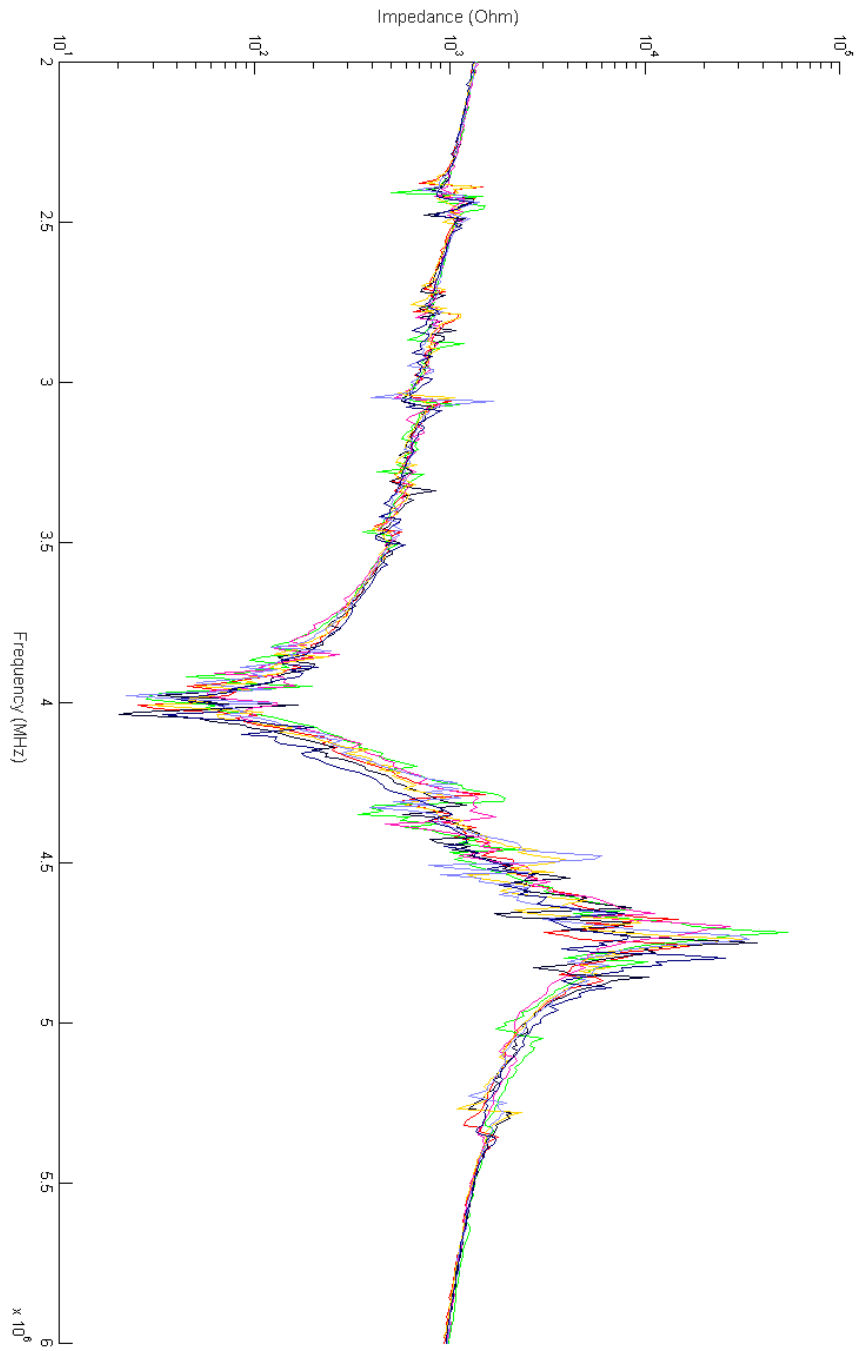

Fabrication of transducers

Test 1. 4 randomly selected transducers that were manufactured in test 1.

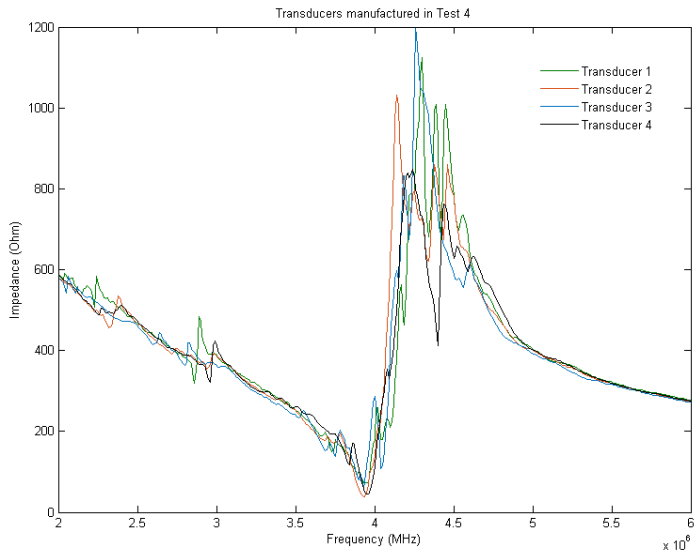


Test 3. 3 randomly selected transducers that were manufactured in test 3.